Development of novel anti-cancer strategies utilizing the zebrafish xenograft model

Chen, Q.

Chapter 4

Photosubstitution in a new trisheteroleptic ruthenium complex inhibits conjunctival melanoma growth in a zebrafish orthotopic xenograft model

Quanchi Chen [1#], Jordi-Amat Cuello-Garibo [2#], Vadde Ramu [2], Yasmin Aydar [1], Yevhen Batsuin,[2] Sharon Bronkhorst [2], Nataliia Beztsinna [2], Lanpeng Chen [1], Xue-Quan Zhou [2], Claudia Schmidt [3], Ingo Ott [3], Martine J. Jager [4], B. Ewa Snaar-Jagalska [1*], Sylvestre Bonnet [2*]

[1] Institute of Biology, Leiden University, Leiden, The Netherlands
[2] Leiden Institute of Chemistry, Leiden University, P.O. Box 9502, 2300 RA Leiden, The Netherlands
[3] Institute of Medicinal and Pharmaceutical Chemistry, Technische Universität Braunschweig, Beethovenstrasse 55, D-38106 Braunschweig, Germany
[4] Department of Ophthalmology, Leiden University Medical Center, Leiden, The Netherlands
# These authors contributed equally to the paper
* Correspondence: b.e.snaar-jagalska@biology.leidenuniv.nl; Tel.: +31-71-527-4980 (E.S.J.) and bonnet@chem.leidenuniv.nl; Tel : +31-71-527-4260 (S.B.);

Manuscript ready for submission to Chemical science

Keywords: Eye, conjunctival melanoma, chemotherapy, photoactivation, zebrafish

Abstract

In vivo data are very rare for ruthenium-based photoactivated chemotherapy (PACT) compounds, a new family of phototherapeutic drugs that are activated *via* ligand photosubstitution. Here a novel trisheteroleptic ruthenium complex ([**2**]$(PF_6)_2$) was generated and its light-activated anticancer properties were validated *in vitro* and in embryonic zebrafish cancer models. The dark toxicity of [**2**]$(PF_6)_2$ was optimized by combining three different ligands with different hydrophobicities, each bound in a bidentate fashion to the metal centre. Upon green light irradiation, one of these ligands, 2-methylthiomethylpyridine (mtmp), was selectively photosubstituted by solvent molecules, thereby releasing the phototoxicity of the heavy metal photoproduct. Fifteen minutes of green light irradiation (21 $mW.cm^{-2}$, 19 $J.cm^{-2}$, 520 nm) led to high phototherapeutic indexes (PI) for this compound, in particular in prostate cancer cells (PC3Pro4) and conjunctival melanoma cells (CRMM1 and CRMM2). The therapeutic potential of [**2**]$(PF_6)_2$ was further evaluated in zebrafish ectopic and orthotopic tumour models of these cell lines. The ectopic model consisted of fluorescent PC3Pro4-, CRMM1-, or CRMM2-mCherry cells, injected intravenously (IV) into zebrafish, that formed perivascular metastatic lesions within four days at the posterior ventral end of caudal hematopoietic tissue (CHT). By contrast, in the orthotopic model, CRMM1- and CRMM2-mCherry cells were injected behind the eye where they developed metastatic lesions. After 24 hours, the engrafted embryos were treated at the maximally-tolerated dose of [**2**]$(PF_6)_2$, which was determined for three different modes of administration: i) incubating the fish in drug-containing water (WA); ii) injecting the compound intravenously (IV) into the fish; or iii) injecting the compound retro-orbitally (RO) into the fish. Optimally, four consecutive PACT treatments were performed on engrafted embryos using 60 min drug-to-light intervals and 90 min green light irradiation (21 $mW.cm^{-2}$, 114 $J.cm^{-2}$, 520 nm). Most importantly, this PACT protocol was not toxic to the zebrafish. In all three ectopic tumour models, [**2**]$(PF_6)_2$ did not significantly diminish the formation of metastatic lesions. However, in both conjunctival melanoma orthotopic tumour models, retro-orbitally administered [**2**]$(PF_6)_2$ significantly inhibited growth of the engrafted cells. Overall, this study represents the first demonstration in zebrafish cancer models of the clinical potential of ruthenium-based photoactivated chemotherapy against conjunctival melanoma.

Introduction

Cisplatin was the first metal-based chemotherapy drug approved by the Food & Drug Administration for the treatment of testicular tumours and ovarian adenocarcinoma, and with the development of carboplatin and oxaliplatin (two derivatives of cisplatin) the use of platinum-based drugs has expanded to the treatment of many different malignancies [1-3]. Although the exact mechanism of action of platinum(II) (Pt) complexes is still debated, it is generally accepted that the ultimate event that induces apoptosis in cancer cells is the binding of the heavy metal centre to DNA after hydrolysis of one or two labile ligand(s) of the metal complex [4]. DNA binding to Pt inhibits DNA replication and transcription, ultimately leading to cell death [5-7]. Spontaneous activation of the drug before it reaches the tumour,

leads to severe side effects in patients treated with platinum drugs, for example hepato- and nephrotoxicity, which limits the clinical efficacy of these compounds and the patients' quality of life [8-10]. Therefore, other metal-based compounds have been considered as anticancer chemotherapy candidates, including those based on ruthenium(II) (Ru) [11]. Although several of these compounds have reached the stage of clinical trials, the general toxicity of metal-based compounds, due to spontaneous activation of a metal-ligand bond before the drug reaches the tumour, remains an issue.

Ruthenium-based PhotoActivated ChemoTherapy (PACT) is a new anticancer phototherapy modality that uses visible light irradiation as an external trigger [12,13]. PACT primarily aims at limiting the biological action of the anticancer drug to the location of the tumour by localized, light-induced activation at the tumour site [14]. Unlike photodynamic therapy (PDT), a clinically-approved anticancer phototherapy method based on the photochemical activation of dioxygen by an excited photosensitizer, PACT relies on an oxygen-independent photochemical bond cleavage reaction. This process generates a molecular species that is more cytotoxic than the (non-activated) prodrug kept in the dark [15-17]. Many examples of PACT agents have been reported in the literature, among which are molecules based on ruthenium [18-20]. Ru-based PACT compounds make use of the versatile and well-understood photochemistry of polypyridyl ruthenium compounds, which, next to energy transfer and electron transfer, comprises light-induced photosubstitution reactions [21]. When photosubstitution occurs, one of the organic ligands bound to the metal is replaced by loosely-bound solvent molecules. In the dark, the ligand to be photosubstituted serves as a protecting group towards the coordination of biomolecules present in cells. After light irradiation, photosubstitution produces an "uncaged" metal compound that, by analogy with cisplatin, acts as an activated drug, as it can bind to biomolecules and induce cell death (Figure 1) [22-24]. For example, blue light-induced photosubstitution of the non-toxic ligand 2-methylthiomethylpyridine (mtmp) in compounds $[Ru(dpp)_2(mtmp)]^{2+}$ ($[\mathbf{1}]^{2+}$, dpp = 4,7-diphenyl-1,10-phenanthroline) and $[Ru(bpy)_2(mtmp)]^{2+}$ ($[\mathbf{3}]^{2+}$, bpy = 2,2'-bipyridine), has recently been demonstrated [25]. These two compounds belong to a wide family of complexes $[Ru(N\text{-}N)_2(L\text{-}L)]^{2+}$, where N-N are non-photocleavable "spectator" polypyridyl ligands, and L-L is a photocleavable chelate [25-29]. Although the photochemistry of this type of complexes is relatively well-understood, two major challenges in their development are on the one hand minimizing the difference between dark and light toxicity, and on the other hand, understanding how the molecular structure relates to the dark toxicity *in vivo*, i.e. the toxicity before photosubstitution takes place. In $[\mathbf{1}]^{2+}$ and $[\mathbf{3}]^{2+}$, both challenges are not met: $[\mathbf{1}]^{2+}$ bears two very hydrophobic dpp chelates that make the complex taken up by cells in large amounts and generate high cytotoxicity before light activation, while $[\mathbf{3}]^{2+}$ bears the much less hydrophobic bpy spectator ligands, as a result of which this compound is too hydrophilic to penetrate significantly into cancer cells, which prevents this compound to show any toxicity even after light activation [24].

We set out to resolve both challenges. First, we designed a new ruthenium complex, $[Ru(dpp)(bpy)(mtmp)]^{2+}$ ($[\mathbf{2}]^{2+}$, Fig. 1), as a compromise between $[\mathbf{1}]^{2+}$ and $[\mathbf{3}]^{2+}$. A single dpp chelate is

expected to alleviate the excessive hydrophobicity and dark toxicity of [**1**]$^{2+}$, while it should increase the cellular uptake and photoinduced anticancer activity of [**3**]$^{2+}$. Second, after demonstration of the excellent phototherapeutic properties of [**2**]$^{2+}$ *in vitro*, this compound was subjected for the first time to *in vivo* efficacy testing and determination of the maximum tolerated dose using zebrafish ectopic and orthotopic tumour models. Zebrafish tumour models are advantageous for anticancer compound development as they allow for fast compound screening *in vivo* with low amounts of compound, compared to rodents, and with better statistics [30-33]. As zebrafish are transparent it is especially easy to activate a phototherapeutic compound by light in the whole body of the animal by simply shining light onto the aqueous solution containing the embryos [34-40]. The transparency of the embryo makes it easy to quantify the relative tumour burden, using engraftment of human cancer cells which stably express red fluorescent protein (RFP). This property has been used for studying PDT [41], as well as photoswitchable inhibitors, allowing analysis before and after light activation [37]. Zebrafish provide a particularly useful animal model for assessing drug toxicity: acute and chronic toxic effects of metal nanoparticles have been measured, with special focus on immunotoxicity, developmental toxicity, neurotoxicity, reproductive toxicity, cardiovascular toxicity, or hepatoxicity [42,43]. Systemic drug toxicity to zebrafish embryos has been well described [44-46]. Th zebrafish model allowed us to investigate for the first time the toxicity of photosubstitutionally active ruthenium compounds in different *in vivo* models of cancer while respecting the 3Rs principles (Reduction, Refinement, Replacement). As zebrafish embryo had not been used for PACT yet, we tested different protocols of compound administration, to find a mode of administration to test anti-cancer efficacy and toxicity. Critically, this work highlights that similarly high efficacies of a PACT compound *in vitro* do not necessarily translate into similarly high efficacies *in vivo*, where the mode of administration of the compound must be carefully optimized for each particular disease model.

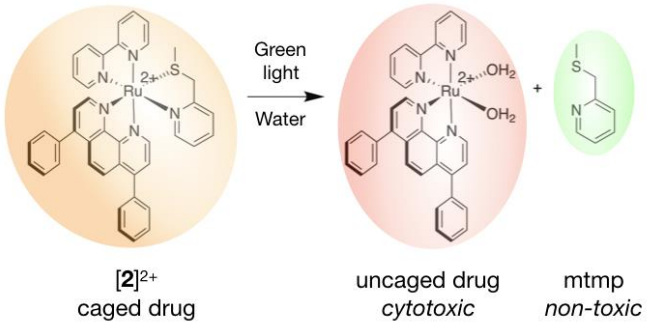

Fig. 1 Activation mechanism of the ruthenium-based PACT compound [**2**]$^{2+}$. Upon green light irradiation, the protecting, non-toxic mtmp ligand is photosubstituted by solvent molecules, which recovers the biomolecule-binding ability of the heavy metal centre, ultimately leading to toxicity and cell death.

Method and Materials

Synthesis

General: the ligands 2,2'-bipyridine (bpy) and 4,7-diphenyl-1,10-phenanthroline (dpp), and the precursor *cis*-[Ru(DMSO)$_4$Cl$_2$], were purchased from Sigma-Aldrich. Potassium hexafluorophosphate (KPF_6) was purchased from Alfa-Aesar. All reactants and solvents were used without further purification. The synthesis of [**1**]Cl$_2$ was described previously [47]. The ligand 2-(methylthiomethyl)pyridine (mtmp) was prepared according to the literature [48]. Electrospray mass spectra (ES MS) were recorded by using a Thermoquest Finnagen AQA Spectrometer and a MSQ Plus Spectrometer. All ^{1}H NMR spectra were recorded on a Bruker DPX-300 or DMX-400 spectrometers. Chemical shifts are indicated in ppm relative to the residual solvent peak.

[Ru(dpp)(DMSO)$_2$Cl$_2$] [**4**]: *cis*-[Ru(DMSO)$_4$Cl$_2$] (500 mg, 1.03 mmol) and bathophenanthroline (343 mg, 1.03 mmol) were heated at reflux in ethanol (35 mL) for 2 h. The reaction was then cooled to room temperature and the solvent volume reduced to *ca*. 10 mL in vacuo. The precipitate that formed upon cooling was filtered, washed with minimal cold ethanol and copious amounts of hexane/diethyl ether, and dried under vacuum. Yield: light-brown solid, 347 mg (0.52 mmol, 51%). ^{1}H NMR (400 MHz, $CDCl_3$) δ 10.19 (d, J = 5.4, 0.9 Hz, 1 H), 10.00 (d, J = 5.6, 0.9 Hz, 1 H), 8.03 (dd, 2 H), 7.89 (d, J = 5.5, 0.9 Hz, 1 H), 7.72 (d, J = 5.6, 0.9 Hz, 1 H), 7.65 – 7.51 (m, 10 H), 3.67 (s, 3 H, 1), 3.62 (s, 3 H, 2), 3.27 (s, 3 H), 2.70 (s, 3 H). ^{13}C NMR (101 MHz, $CDCl_3$) δ 155.72, 152.34, 149.95, 148.98, 135.93, 135.79, 129.81, 129.68, 129.13, 128.73, 128.27, 125.49, 125.36, 125.30, 125.23, 47.15, 46.52, 45.49, 44.37.

[Ru(dpp)(ox)(mtmp)] [**5**]: [**4**] (300 mg, 0.45 mmol) and sodium oxalate (84.5 mg, 0.65 mmol) were heated at reflux in water (15 mL) for 1 h. The reaction was then cooled to room temperature and added to a hot (60 °C) solution of 2-[(methylthio)methyl]pyridine (63 mg, 0.45 mmol) in ethylene glycol (15 mL). The resulting mixture was heated at reflux for 3 h, cooled to room temperature and then added dropwise to 50 mL of stirring water. After 30 minutes, the precipitate was filtered through a 1 µm Micropore membrane. The solids were washed with copious amounts of water and minimal acetone before drying thoroughly under vacuum. Mixture of isomers was separated in silica column (Rf = 0.3) in DCM/ CH_3OH (2-20% CH_3OH). Only one isomer was isolated. Yield: dark red powder, 144 mg (0.21 mmol, 71%). ^{1}H NMR (400 MHz, $CDCl_3$) δ 9.63 (d, J = 5.6, 0.9 Hz, 1H), 9.34 (d, J = 5.4, 0.9 Hz, 1H), 8.08 (dd, J = 9.4, 0.9 Hz, 2H), 7.81 (d, J = 5.3 Hz, 1H), 7.64 – 7.47 (m, 11H), 7.43 – 7.36 (m, 2H), 6.81 (d, 1H), 6.59 (t, J = 6.1, 2.4 Hz, 1H), 4.66 (dd, 2H), 2.45 (s, 3H). ^{13}C NMR (101 MHz, $CDCl_3$) δ 168.86, 167.83, 163.08, 153.42, 152.04, 151.05, 149.48, 148.15, 145.53, 136.37, 136.29, 134.29, 129.96, 129.78, 129.53, 129.35, 129.21, 129.17, 129.03, 128.39, 125.91, 125.48, 124.44, 123.14, 122.34, 45.79, 16.12. Anal. Calcd for $C_{33}H_{25}N_3O_4RuS{\cdot}3H_2O$: C, 55.45; H, 4.37; N, 5.88 Found: C, 56.08; H, 4.56; N, 5.46.

[Ru(dpp)(bpy)(mtmp)](PF$_6$)$_2$ [**2**](PF$_6$)$_2$: [**5**] (140 mg, 0.211 mmol) was suspended in acetonitrile (3 mL) and then perchloric acid 1 M (3 mL) was added. After refluxing for 1 h, a red-brown solution of the Ru-

solvate was obtained and after cooling it was poured on 15 mL stirring water. The solid that precipitated was filtered and dried to yield the crude orange $[Ru(dpp)(mtmp)(CH_3CN)_2](ClO_4)_2$ complex. The intermediate was dissolved in an ethylene glycol solution (15 mL) containing the bpy ligand (33 mg, 0.211 mmol) and heated at 100 °C for 6 h. The deep red mixture was cooled to room temperature and poured on stirring aqueous potassium hexafluorophosphate to precipitate the crude complex as the hexafluorophosphate salt. Configurational isomers were resolved by column chromatography on silica DCM/CH_3OH 95:5. Three fractions were obtained from a long orange band (Rf ~ 0.5), from which only the last fraction contained a pure isomer (3.2 mg, 1.5%) (Isomer B, [**2b**]$(PF_6)_2$). A mixture of isomers A/B in a ration 0.23:1 has been used for photochemical analysis and biological testing, further referred to as [**2**]$(PF_6)_2$ (60 mg, 28%). ^{1}H NMR (400 MHz, CD_3CN) δ 9.63 (d, J = 5.5 Hz, 1HB), 9.39 (d, J = 5.7 Hz, 1HA), 8.61 (d, J = 8.2 Hz, 1HB), 8.58 – 8.51 (m, 2HA), 8.43 (d, J = 8.1 Hz, 1HB), 8.31 (dd, J = 8.0, 1.5 Hz, 1HB), 8.29 – 8.23 (m, 1HB + 1HA), 8.22 – 8.14 (m, 2HB + 2HA), 8.14 – 8.03 (m, 3HA), 8.02 (d, J = 5.5 Hz, 1HB), 7.99 (d, J = 5.5 Hz, 1HB), 7.93 (ddd, J = 7.8, 6.5, 1.5 Hz, 1HB), 7.86 (td, J = 7.8, 1.6 Hz, 1HA), 7.81 – 7.51 (m, 15HB + 15HA), 7.48 (dd, J = 5.9, 1.5 Hz, 1HA), 7.32 (ddd, J = 7.1, 5.6, 1.3 Hz, 1HA), 7.24 (d, J = 5.5 Hz, 1HB), 7.17 (td, J = 7.2, 5.6, 1.4 Hz, 1HB + 1HA), 6.98 (ddd, J = 7.7, 5.8, 1.6 Hz, 1HB), 4.82 (d, J = 16.5 Hz, 1HB), 4.74 (d, J = 16.7 Hz, 1HA), 4.28 (dd, J = 16.6, 4.8 Hz, 1HB + 1HA), 1.59 (s, 3HB), 1.32 (s, 3HA). ^{13}C NMR (101 MHz, CD_3CN) δ 162.96, 162.63, 158.56, 157.73, 153.51, 153.33, 153.09, 152.90, 151.98, 150.77, 150.61, 150.05, 149.66, 148.72, 139.46, 138.67, 138.55, 136.62, 136.53, 130.79, 130.70, 130.13, 130.06, 129.20, 127.78, 127.26, 127.19, 127.12, 126.92, 125.86, 125.59, 125.55, 124.93, 45.36, 17.04. High Resolution ES MS m/z (calcd): 364.57519 (364.57446, [2]2+). Anal. Calcd for $C_{41}H_{33}F_{12}N_5P_2RuS$: C, 48.34; H, 3.26; N, 6.87 Found: C, 48.21; H, 3.41; N, 6.82.

Photochemistry: determination of the photosubstitution and singlet oxygen generation quantum yields

When monitoring photoreactions with UV-vis and mass spectrometry, a Cary 50 Varian spectrometer equipped with temperature control set to 298 K and a LED light source (λ_{ex} = 521 nm, with a Full Width at Half Maximum of 33 nm) with a photon flux of $6.21 \cdot 10^{-8}$ mol·s^{-1} was used. The irradiation experiments were performed in a quartz cuvette containing 3 mL of solution. A stock solution of the desired complex was prepared in CH_3CN, which was then diluted in the cuvette to a working solution concentration (36 µM). The sample was deaerated 15 min by gentle bubbling of dinitrogen and the atmosphere was kept inert during the experiment by a gentle flow of dinitrogen on top of the cuvette. A UV-vis spectrum was measured every 30 s for the first 10 min, every 1 min for the next 10 min, and eventually every 10 min until the end of the experiment. Data were analysed with Microsoft Excel and Glotaran as follows: Upon light irradiation, a complex RuL converts into a complex RuY by photosubstitution of a ligand (L) by a solvent molecule (Y). Considering that both metal complexes are thermally stable, the quantum yield of the photosubstition reaction Φ_{PR} can be calculated by monitoring the photoreaction with UV-vis spectroscopy. As explained in detail by Bahreman and Bonnet

[49], when the irradiation is performed at a wavelength that is not an isosbestic point, the Φ_{PR} can be obtained from the slope of a plot of the number of mol of RuL (n_{RuL}) *vs.* the total number of mol of photons absorbed by RuL from t_0 till t_i (Q_i). Q_i is calculated according to Equation 1:

$$Q_i(t) = \sum_{t=0}^{i} q_i \qquad \textit{Equation 1}$$

where q_i is the moles of photons absorbed by RuL between two consecutive UV-vis measurements at t_{i+1} and t_i ($\Delta t = t_{i+1} - t_i$). q_i is calculated according to Equation 2:

$$q_i = \left(\frac{(A_{RuL})_{ave}}{(A_e)_{ave}}\right)_i \cdot (1 - 10^{-3\cdot(A_e)_{ave}}) \cdot \varphi \cdot \Delta t \qquad \textit{Equation 1}$$

where $(A_{RuL})_{ave}$ is the average of the absorbance due to RuL between two consecutive UV-vis measurements, $(A_e)_{ave}$ is the average of the absorbance of the solution at the irradiation wavelength between two consecutive UV-vis measurements, $(1 - 10^{-3\cdot(A_e)_{ave}})$ is the probability of absorption of a photon when the irradiation comes from the top of the quartz cuvette and goes through 3 cm pathlength, while all absorbances are measured perpendicularly through a 1 cm pathlength, and ϕ is the photon flux of the irradiation source at the irradiation wavelength.

The value of $(A_{RuL})_{ave}$, and by extension n_{RuL}, was calculated by modelling the evolution of the UV-vis spectra *vs.* time using the Glotaran software. We fitted hence the time-dependent evolution of the UV-vis spectroscopy data to a kinetic model based on first-order laws, obtaining two output data sets that can be used for the calculation of Φ_{PR}. The first dataset is a collection of globally fitted absorption spectra of the starting complex and the photoproduct, which makes possible the calculation of the molar extinction coefficient of all the species from that of the starting reagent (Fig. S1a). The second dataset is the modelled evolution of the relative fractions of the two ruthenium species *vs.* irradiation time, here as well according to global fitting (Fig. S1b). From the time evolution of these fractions and the molar absorption coefficient of all species, the time evolution of n_{RuL} can be calculated, as well as Q_i. The slope of the plot of n_{RuL} *vs.* Q_i (Fig. S1c) gives the quantum yield of the reaction.

Singlet oxygen quantum yield measurements were performed by direct spectroscopic detection of the 1275 nm emission, as described by Meijer *et al* [25].

Attached cell culture

Human conjunctival malignant melanoma cell lines CRMM1 and CRMM2, isolated by Nareyeck et al [50], were cultured in F12 Kaighn's modified medium (Hyclone, cat# SH30526.01) supplemented with 10% fetal bovine serum (FBS; Gibco). CM2005.1 established by Keijser et al [51] was cultured in RPMI 1640, Dutch Modified (Life Technologies, cat# 22409-015), supplemented with 10% fetal bovine serum (FBS; Gibco), 3 mM L-glutamine (1%, Life Technologies cat# 35050-038). Human uveal melanoma cell lines OMM1 (provided by Prof. Dr. G.P.M Luyten) [52], OMM2.5, and MEL270 (provided by Dr. B.R. Ksander) [53] were cultured in Ham's F12 medium (Sigma-Aldrich, cat# N3790) supplemented with 10%

FCS. Stable fluorescent CRMM1 and CRMM2 cell lines were generated using lentivirus expressing both tandem dimer (td)Tomato and Blasticidin-S, as previously described [54]. PC3Pro4 (provided by Dr. Gabriel van der Pluijm) was cultured in DMEM (Sigma-Aldrich, cat# 32160801) supplemented with 10% FCS. Human lung carcinoma A549 was distributed by the European Collection of Cell Cultures (ECACC), and purchased from Sigma Aldrich, cultured in DMEM (Sigma-Aldrich, cat# 32160801) supplemented with 10% FCS. Cells were cultured in either 25 cm^2 or 75 cm^2 flasks and split at 70-80% confluence. The flasks were incubated in a normoxic incubator at 37 °C at 5.0% CO^2 in a PHCbi O^2/CO^2 incubator, MCO-170M). The medium was refreshed twice a week. Cells used in all biological experiments were cultured for not more than eight weeks. Trypsin and Opti-MEM® (without phenol red) were purchased from Gibco® Life Technologies. Trypan blue (0.4% in 0.81% sodium chloride and 0.06% potassium phosphate dibasic solution) was purchased from Bio-Rad. Plastic disposable flasks and 96-well plates were obtained from Sarstedt. Cells were counted using a Bio-Rad TC10 automated cell counter with Bio-Rad Cell Counting Slides.

Spheroids cell culture and CellTiter-Glo 3D cell viability assay

A549 (500 cells/well) within 100 µL OptiMEM (Gibco® Life Technologies, cat# 11058021) were seeded in the low-attachment 96 well plates (Corning Spheroid microplate 4515) and incubated in normoxia (21% O_2). After 24 h, 100 µL/well of diluted [**2**]$(PF_6)_2$ with six different concentrations in OptiMEM or OptiMEM for control was added into each well and the cells were further incubated for another 24 h (drug-to-light interval). 100 µL of medium was pipetted out from each well and 100 µL/well of new OptiMEM was added. Then, the plates for [**2**]$(PF_6)_2$ treatment with light activation and vehicle with light activation groups were irradiated with green light (21 $mW.cm^{-2}$, 15 min, 19 $J.cm^{-2}$, 520 nm) and the plates for [**2**]$(PF_6)_2$ treatment with no light activation and vehicle with no light activation groups were put in the dark box. After treatment, all plates were put back in the incubator for 48 h. Before the CellTiter-Glo 3D cell viability assay, the plates were taken out from the incubator and left out for 20 min to reach the room temperature. 100 µL medium was taken out from each plate and 100 µL of CellTiter Glo 3D was added per well. The plates were put on the shaker for 5 min and left the plates at room temperature without shaking for 25 min. The luminescence of the plates was read by Tecan reader.

Cellular uptake

Cell uptake studies for complexes [**1**]Cl_2 and [**2**]$(PF_6)_2$ were conducted on A549 lung cancer cells. $1.6 \cdot 10^6$ cells were seeded at t = 0 h in Opti-MEM complete (10 mL) in a 75 cm^2 T-flask. At t = 24 h the media was aspirated and cells were treated with solutions of [**1**]Cl_2, [**2**]$(PF_6)_2$ to give a final concentration at the EC_{50} in the dark (3.4 and 65µM, respectively) in a total volume of 10 mL. After 24 h of drug incubation at 37 ºC and 21% O_2, the medium was aspirated and the cells were washed twice with PBS (5 mL). Then, the cells were trypsinized (2 mL), suspended with Opti-MEM (8 mL), and centrifuged (1200

rpm, 4 min). After aspiration of the supernatant, the cells were re suspended in PBS (1 mL) and counted. After a second centrifugation, the supernatant was discarded. For metal and protein quantification, the pellets were resuspended in demineralized water (250 µL) and lysed for 30 min by ultrasonication. The protein content of lysates was determined by the Bradford method, and the ruthenium content was determined by Atomic Absorption Spectroscopy.

A contrAA 700 high-resolution continuum-source atomic absorption spectrometer (Analytik Jena AG) was used. Pure samples of the respective complex were used as standard and calibration was done in a matrix-matched manner (meaning all samples and standards were adjusted to the same cellular protein concentration of 1.0 mg/mL by dilution with distilled water if necessary). Triton-X 100 (1%, 10 µL) as well as nitric acid (13%, 10 µL), were added to each standard sample (100 µL). Samples were injected (25 µL) into coated standard graphite tubes (Analytik Jena AG) and thermally processed as previously described by Schatzschneider et al.[55] Drying steps were adjusted and the atomization temperature set to 2400 °C. Ruthenium was quantified at a wavelength of 349.90 nm. The mean integrated absorbances of double injections were used throughout the measurements. The data from two independent biological replications were used to obtain the uptake values shown in Table 2.

Cell irradiation setup

The cell irradiation system consisted of a Ditabis thermostat (980923001) fitted with two flat-bottomed microplate thermoblocks (800010600) and a 96-LED array fitted to a standard 96-well plate. The λ=520 nm LED (OVL3324), fans (40 mm, 24 V DC, 9714839), and power supply (EA PS 2042-06B) were obtained from Farnell as reported in our previous publication [56].

Cytotoxicity assay

At day 0, cells were detached using 1 mL of trypsin, resuspended in 4 mL of media and transferred to a 15 mL corning falcon tube. Cells were counted using trypan blue and BioRad® TC20™ automated cell counter (Figure 11). Dilutions of 6000 (CRMM1), 6000 (CRMM2), 8000 (CM2005.1), 6000 (OMM1), 6000 (OMM2.5), 6000 (MEL270) 6000 (A549), and 6000 (PC3Pro4) cells/well were calculated from each cell suspension at a final volume of 6 mL. The cell suspensions were transferred to a 50 mL reservoir and 100 µL of each cell line was seeded at the aforementioned cell densities in triplicate in six 96-well plates. Boarder wells were intentionally filled with PBS media to avoid boarder effects. After 24 h, the cells were treated with [**2**]$(PF_6)_2$ with six different concentrations. After 24 h of post treatment the cells were exposed to the green light for 15 min (21 mW/cm^2, 19 J.cm^{-2}, 520 nm). The dark control plate was kept under dark conditions. Then cells were incubated for another 48 h before fixing them with trichloroacetic acid (10% w/w) solution. The fixed cells were kept at 4℃ for 48h, when TCA was washed

out with distilled water before adding the sulphorhodamin B (SRB) (0.6 % SRB) dye. The SRB dye was washed out after 30 minutes and plates were air dried overnight. Next day, the dye was dissolved using Tri-base (0.25%) and absorbance of SRB at 510 nm was recorded from each well using a Tecan plate reader. The SRB absorbance data was used to calculate the fraction of viable cells in each well (Excel and GraphPad Prism software). The absorbance data were averaged from triplicate wells per concentration. Relative cell viabilities were calculated by dividing the average absorbance of the treated wells by the average absorbance of the untreated wells. Three independent biological replicates were completed for each cell line (three different passage numbers per cell line). The average cell viability of the three biological replicates was plotted versus log(concentration) [μM], with the SD error of each point. By using the dose–response curve for each cell line under dark- and irradiated conditions, the effective concentration (EC50) was calculated by fitting the curves to a non-linear regression function with a fixed maximum (100 %) and minimum (0 %) (relative cell viability) and a variable Hill slope [57].

Flow Cytometry

CRMM1 (10000/well) cells were seeded into an 8-well chamber in Opti-MEMTM (Gibco, Reduced Serum Medium, no phenol red) with 2.5% FBS (Gibco). After 24 h incubation, 4.3 μM of [**2**]$(PF_6)_2$ was added into the medium. 24h later, wells were washed and new drug-free medium was added. The cells were exposed to green light (21 mW/cm^2, 19 J.cm^{-2}, 520 nm) for 15 min and incubated for 48 h. Medium of all wells was collected and wells were washed with PBS and lysed by 500 μL trypsin for 3 min. Collected medium was added to the wells with lysed cells, mixed and centrifuged for 2000 rpm, 3 min. After washing, cells were resuspended in 200 μL of 1X binding buffer. Next, 5 μL of Annexin-V-FITC and 5 μL of Propidium Iodide were added to each well and left for 15 min at room temperature. 200 μL of each sample was added to a well in a 96-well plate, and used for FACS measurement.

Zebrafish maintenance, tumour cells implantation and tumour analysis

Zebrafish lines were kept in compliance with the local animal welfare regulations and European directives. The study was approved by the local animal welfare committee (DEC) of Leiden University (Project: “Anticancer compound and target discovery in zebrafish xenograft model”. License number: AVD1060020172410). The Zebrafish Tg(fli1: GFP/Casper) [58] were handled in compliance with local animal welfare regulations and maintained according to standard protocols (www.ZFIN.org).

For cancer cell injection, two days post-fertilization (dpf), dechorionated zebrafish embryos were anaesthetized with 0.003% tricaine (Sigma) and plated on a 10cm Petri dish covered with 1.5% of solidified agarose. PC3Pro4, CRMM1 and CRMM2 cells were suspended in PBS containing 2% polyvinylpyrrolidone (PVP; Sigma-Aldrich) with a concentration of 50,000 cells/μl and loaded into borosilicate glass capillary needles (1 mm O.D. × 0.78 mm I.D.; Harvard Apparatus). In the ectopic model, 200 mCherry fluorescent PC3Pro4 or (td)Tomato fluorescent CM cells were injected into the

Duct of Cuvier at 2 dpf, which led to dissemination through the blood circulation and outgrowth in the head and tail. In orthotopic tumour model, 100 (td)Tomato fluorescent CRMM1 or CRMM2 cells were injected retro-orbitally in 2 dpf embryos using a Pneumatic Picopump and a manipulator (WPI). After injection, the embryos were incubated in a 34 ˚C incubator. Images were acquired at 1-, 2-, 4- and 6-days post injection (dpi) with a Leica M165 FC stereo fluorescence microscope. Tumour growth was quantified by calculating the total fluorescence intensity and area with the ZF4 pixel counting program (Leiden). Each experiment was performed at least 3 times with a group size of >30 embryos.

Maximum tolerated dose (MTD) for wild-type zebrafish and tumour cell-injected zebrafish

For determining the MTD of the water administration (WA) of the [**2**]$(PF_6)_2$ solution in wild type zebrafish, solutions of 0.1 µM, 0.25 µM, 0.5 µM, 1 µM, 2 µM were made before the experiment. At 2.5, 3.5, 4.5, 5.5 dpf, [**2**]$(PF_6)_2$ was added to the fish water and maintained for 12 h. At 3, 4, 5, 6 dpf, the fish water was refreshed and after 1 h, embryos were exposed to green light for 90 min (21 $mW.cm^{-2}$, 114 $J.cm^{-2}$, 520 nm). For the IV and RO administration, [**2**]$(PF_6)_2$ solution (50 µM, 100 µM, 200 µM, 300 µM, 500 µM) was made before the experiment. At 3, 4, 5, 6 dpf, 1nl of [**2**]$(PF_6)_2$ was injected via the dorsal vein or the RO site and maintained for 1 h. Embryos were exposed to green light for 90 min (21 $mW.cm^{-2}$, 114 $J.cm^{-2}$, 520 nm). The images of treated and wild type embryos at 6dpf were taken using a DFC420C camera coupled to a Leica MZ16FA fluorescence microscope. In order to determine the MTD of tumour cell-bearing zebrafish, 90 min green light activation (21 $mW.cm^{-2}$, 114 $J.cm^{-2}$, 520 nm) was performed according to the same procedure, after [**2**]$(PF_6)_2$ was delivered by WA, IV and RA administration as described above for the wild type embryos.

The antitumour efficacy of [2]$(PF_6)_2$ by WA, IV and RO in zebrafish ectopic and orthotopic tumour models

Fluorescent PC3Pro4 cells were injected at 2 dpf into the Duct of Cuvier (ectopic model) and [**2**]$(PF_6)_2$ was delivered by WA and IV administration with or without light treatment as described in 5.9. Fluorescent CRMM1 or CRMM2 cells were injected at 2 dpf into the Duct of Cuvier (ectopic model) and behind the eye (orthotopic model) and [**2**]$(PF_6)_2$ was delivered by WA IV and RO administration with or without light treatment as described in 5.9. For the WA administration, the 0.5 µM [**2**]$(PF_6)_2$ solution was added to the tumour cells-injected zebrafish at 2.5, 3.5, 4.5, 5.5 dpf and maintained for 12 h. At 3, 4, 5, 6 dpf, the fish water was refreshed, and after 1 h, embryos were exposed to green light for 90 min (21 $mW.cm^{-2}$, 114 $J.cm^{-2}$, 520 nm). For the IV and RO administration, 1 nL of 200 µM [**2**]$(PF_6)_2$ solution was injected via the dorsal vein or the RO site at 3, 4, 5, 6 dpf. After 1 h interval, the embryos were exposed to green light for 90 min (21 $mW.cm^{-2}$, 114 $J.cm^{-2}$, 520 nm). After treatment, the embryo images were acquired with a Leica M165 FC stereo fluorescence microscope. Tumour growth was

quantified by calculating the total fluorescence intensity and area with the ZF4 pixel counting program (Leiden). Each experiment was performed at least 3 times with a group size of >30 embryos.

TUNEL assay

The zebrafish larvae were fixed overnight with 4% PFA at 4 ˚C. Embryos were washed in PBST for five minutes and dehydrated by a graded methanol series until reaching 100% methanol. Embryos were stored at -20 ˚C for further use. Embryos were gradually rehydrated in PBST (25%, 50%, 75%), washed twice for 10 minutes with PBST and digested by proteinase K (Roche) solution in PBST (10 µg/ml) at 37 ˚C for 40 minutes. After two washes in PBST, embryos were post-fixed in 4% PFA for 20 minutes. After washing them again twice in PBST for 10 minutes, 50 µl of TdT reaction mix (Roche) was added to the embryos. Embryos were overnight incubated with the TdT at 37 ˚C (in the dark). The reaction was stopped by three 15 min washes with PBST at room temperature and embryos were used for high-resolution imaging. Embryos were placed on glass-bottom petri dishes and covered with 1% low melting agarose containing 0.003% tricaine (Sigma). Imaging was performed using the Leica SP8 confocal microscope. The images were processed with ImageJ software. Each experiment was performed 3 times with a group size of 10 embryos.

Statistical analysis

Determination of the EC_{50} concentrations in vitro was based on a non-linear regression analysis performed using GraphPad Prism Software. Results are presented as means ± SD from three independent experiments. Significant differences were detected by one-way ANOVA followed by Dunnett's multiple comparisons test implemented by Prism 8 (GraphPad Software, La Jolla, CA, USA). A p-value < 0.05 was considered statistically significant, *: p <0.05, **: p<0.01, ***: p<0.001.

Results and discussion

Synthesis and photoreactivity

The synthesis of [**2**]$^{2+}$ is more challenging than that of complexes such as [**1**]$^{2+}$ or [**3**]$^{2+}$ because [**2**]$^{2+}$ is a tris-heteroleptic compound, i.e. it bears three different bidentate ligands that need to be coordinated to the metal in a controlled fashion (Fig. 2). With most generic synthetic routes, ligand scrambling occurred, i.e. [**2**]$^{2+}$ was obtained with traces of [Ru(dpp)(mtmp)$_2$]$^{2+}$, [Ru(bpy)(mtmp)$_2$]$^{2+}$, [**1**]$^{2+}$, or [**3**]$^{2+}$, that were very difficult to remove. The synthesis of [**2**](PF$_6$)$_2$ was hence adapted from a novel method developed by Keyes *et al* [59] that involved the sequential coordination, in this order, of dpp, mtmp, and bpy. The novelty of this method relies on the use of an intermediate oxalate ligand (ox^{2-}) during the coordination of the second (mtmp) chelate. This negatively-charged chelate prevents the formation of species where two identical ligands coordinate to the metal even when one equivalent of mtmp is

used. After purification of the [Ru(dpp)(mtmp)(ox)] ([**5**]) intermediate complex, oxalate was removed selectively by $HClO_4$ treatment in acetonitrile, after which the last chelate (bpy) was reacted to afford, after counter anion metathesis, [**2**]$(PF_6)_2$. Due to the dissymmetry of mtmp and the tri-heteroleptic nature of the final complex, two configurational isomers are expected: one having the sulfur donor atom *trans* to bpy and another having the sulfur donor atom trans to dpp. These isomers were detected by ^{1}H NMR and initially separated by column chromatography. Isomer [**2a**]$(PF_6)_2$ was slightly contaminated with [Ru(dpp)$(bpy)_2$]$(PF_6)_2$, while isomer [**2b**]$(PF_6)_2$ was pure according to ^{1}H NMR but obtained in a low yield (<2%). Later on, as no difference in reactivity could be observed between both isomers, mixtures of [**2a**]$(PF_6)_2$ and [**2b**]$(PF_6)_2$ deprived of any other impurities were prepared and further used in biological studies; it is designated below as [**2**]$(PF_6)_2$.

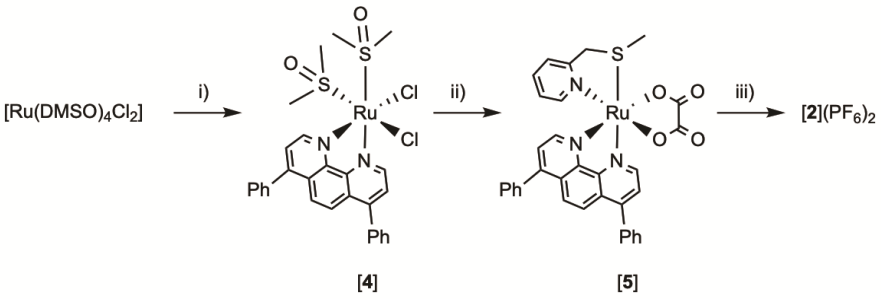

Figure 2 Synthesis of tris-heteroleptic compound [Ru(dpp)(bpy)(mtmp)]$(PF_6)_2$ ([**2**]$(PF_6)_2$). Conditions: i) 1.0 eq. dpp, EtOH, reflux 2 h, Y = 51%. ii) a) 1.5 eq. $Na_2C_2O_4$; water, reflux 1 h; b) 1.0 eq. mtmp, ethylene glycol, reflux 3 h; c) water; Y = 71%. iii) a) 1 M $HClO_{4(aq)}$/CH_3CN 1:1, reflux 1 h, b) 1.0 eq. bpy, ethylene glycol, 100 °C, 6 h; 3) aqueous KPF_6; Y = 28%.

The photoreactivity of [**2**]$(PF_6)_2$ was studied by UV-vis spectroscopy in CH_3CN. The spectrum of a solution of [**2**]$(PF_6)_2$ irradiated for 20 minutes with green light (521 nm, 14 mW.cm^{-2}) showed an increase of the intensity of the metal-to-ligand charge-transfer (MLCT) band between 400-430 nm, and a decrease in the valley at 344 nm with clear isosbestic points at 363 and 440 nm (Fig. 3). After 15 minutes, when the reaction reached the steady state, mass spectrometry showed peaks at m/z = 140.3 and 336.3, corresponding to the free caging ligand {mtmp+H}$^+$ (calcd m/z = 140.1) and [Ru(bpy)$(Ph_2hen)(CH_3CN)_2]^{2+}$ (calcd m/z = 336.1). No traces of bpy, dpp, or of any ruthenium complex resulting from the photosubstitution of one of the two bis-imine ligands, was observed by mass spectrometry. There was also no trace of the starting complex [**2**]$^{2+}$, confirming the selective and complete photosubstitution of mtmp upon light irradiation in deaerated CH_3CN, to produce [Ru(dpp)(bpy)$(MeCN)_2]^{2+}$ as sole photosubstitution product. The photosubstitution quantum yield, measured by UV-vis spectroscopy was found to be 0.111 in these conditions (Fig. S1). The excited states of [**2**]$^{2+}$ do not necessarily deactivate only via photosubstitution and non-radiative decay; reaction with ground state oxygen to produce singlet oxygen ($^1O_2$) may happen, too, as described in PDT type II [60-62]. Hence, the quantum yield for the generation of $^1O_2$ (Φ_Δ) was experimentally determined by direct detection of the 1274 nm near-infrared phosphorescence of $^1O_2$ in an air-equilibrated CD_3OD solution

of [**2**](PF$_6$)$_2$. Under blue light irradiation (450 nm) using [Ru(bpy)$_3$]Cl$_2$ as reference (Φ_Δ = 0.73) [63], a Φ_Δ value of 0.096 was found for [**2**]$^{2+}$, which is slightly higher than for [**1**]$^{2+}$ (Φ_Δ = 0.020 in the same conditions), but much lower than PDT sensitizers such as Photofrin (0.90) [64], Foscan (0.43) [65], or TLD-1433 (1.0) [66]. Overall, the low Φ_Δ value and a rather high photosubstitution quantum yield make of [**2**]$^{2+}$ a promising PACT agent, provided it can enter cancer cells before light irradiation take place.

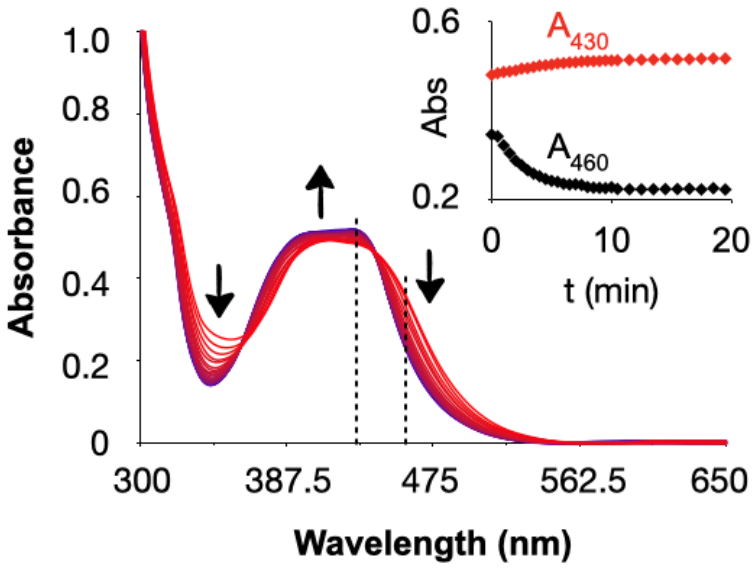

Figure 3 Evolution of the UV-vis spectrum of an acetonitrile solution of [**2**](PF$_6$)$_2$ (36 µM) upon green light irradiation (521 nm, 14 mW.cm^{-2}, photon flux 6.2×10^{-8} mol.s^{-1}) under inert atmosphere. Insert: black and red dots represent the evolution of the absorbance at 460 nm and 430 nm, respectively (dashed lines in the spectrum), vs. irradiation time.

Cellular uptake and cytotoxicity *in vitro*

Considering the good photosubstitution properties of [**2**]$^{2+}$, its cytotoxicity was first tested in the dark and upon green light activation in a human lung cancer cell line (A549) where the two known analogues [**1**]$^{2+}$ and [**3**]$^{2+}$ had already been evaluated [47]. The protocol is detailed in Hopkins *et al.* [67]. The effective concentrations (EC$_{50}$), defined as the compound concentration (in µM) that reduces cell viability by 50% compared to untreated cells, are shown in Table 1. In the dark, the EC$_{50}$ value was 59 µM for [**2**]$^{2+}$, which is intermediate between that found, in the same conditions, for [**1**]$^{2+}$ (3.4 µM) and for [**3**]$^{2+}$ (>100 µM) [14]. After 15 minutes green light irradiation (520 nm, 21 mW.cm^{-2}, 19 J.cm^{-2}), the EC$_{50}$ value decreased to 6.5 µM or [**2**]$^{2+}$, respectively, which is also intermediate between the 0.62 µM and >150 found for [**1**]$^{2+}$ and [**3**]$^{2+}$, respectively (Fig. 4). As suggested by Lameijer et al, validating a compound as either a PACT agent or a PDT agent requires comparing the photoindexes (PI), rather than the EC$_{50}$ values [68]. The photoindexes (PI) value for [**2**]$^{2+}$ (9.1) was twice higher than for [**3**]$^{2+}$ (5.5), which suggested that the compound design was successful. Qualitatively, cytotoxicity is closely related to cellular uptake and subcellular localization, which are in turn closely related to the lipophilicity of the

prodrug [69]. Typically, the presence of more phenyl groups results in an increase of lipophilicity [70]. The intermediate lipophilicity of [**2**]$^{2+}$ obtained by balancing the number of dpp and bpy ligands, significantly decreased its dark toxicity, compared to [**1**]$^{2+}$, while keeping its cytotoxicity after light activation much higher than for [**3**]$^{2+}$. To verify quantitatively that this effect was related to drug uptake, A549 cells were treated for 24 h with [**1**]Cl_2 and [**2**]$(PF_6)_2$ at their EC_{50} concentrations (3.4 and 65 µM, respectively), counted, lyzed, after which the ruthenium content was measured using ICP-MS (Table 1). In such conditions, the cellular uptake of [**2**]$^{2+}$ was found almost equal to that of [**1**]$^{2+}$, although the concentration used for treatment was 20 times higher. Similar experiments with [**3**]$^{2+}$ had demonstrated that this compound was not taken up by A549 cells because of its too high hydrophilicity [14]. Thus, the intermediate lipophilicity of [**2**]$^{2+}$, between that of [**1**]$^{2+}$ and [**3**]$^{2+}$, indeed allowed for moderating cellular uptake, which kept the dark toxicity low while not jeopardizing the toxicity after light activation (Table 2). Such balanced lipophilicity also allowed the compound to penetrate 3D multicellular tumour spheroids of the same cell line (A549). In such conditions, the activity of [**2**]$^{2+}$ remained significantly improved upon light irradiation, with EC_{50} values in the dark and after light irradiation (520 nm, 21 mW.cm^{-2}, 19 J.cm^{-2}) of 172.9 and 70.9 µM, respectively. Most importantly, the viability of the tumour spheroid was almost eradicated at 300 µM upon light irradiation, which highlights the excellent phototoxicity of this compound also in a 3D environment.

Table 1 Cytotoxicity expressed as cell growth inhibition effective concentrations (EC_{50} with 95% confidence intervals, in µM) of [**1**]Cl_2, [**2**]$(PF_6)_2$ and in lung (A549) and prostate (PC3Pro4) cancer cell lines, in the dark and upon green light irradiation (21 mW.cm^{-2}, 15 min, 19 J.cm^{-2}, 520 nm).

Cell line	Light dose (J.cm^{-2})	[**1**]Cl_2			[**2**]$(PF_6)_2$			[**3**]Cl_2		
		EC_{50}	95%CI	PI	EC_{50}	95%CI	PI	EC_{50}	95%CI	PI
A549	0	3.4	-0.76 0.97		59	-13 17		>150	-	-
	19	0.62	-0.11 0.14	5.5	6.5	-1.8 2.4	9.1	>150	-	-
PC3Pro4	0	4.7	-0.30 0.32		142	-52 83		>150	-	-
	19	0.79	-0.027 0.028	6.0	3.2	-0.54 0.65	45	>150	-	-

Table 2 Cellular uptake of [**1**]Cl_2 and [**2**]$(PF_6)_2$ in A549 cells upon treatment near the dark EC_{50} value.

	[**1**]Cl_2	[**2**]$(PF_6)_2$
Treatment concentration (µM)	3.4	65
Cellular uptake (nmol Ru/mg of cell protein)	2.11 ± 0.12	2.12 ± 0.33

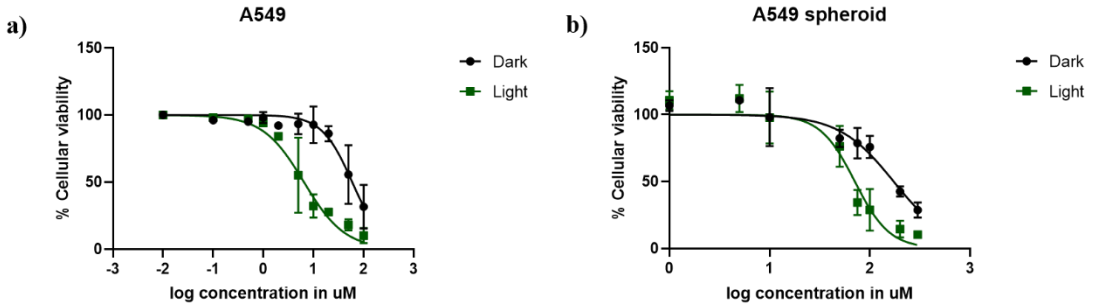

Figure 4 Dose-response curves for A549 cells treated with [**2**](PF$_6$)$_2$, and irradiated with green light (520 nm, 15 min, 21 mW.cm^{-2}, 19 J.cm^{-2}) 24 h after treatment (green data points) or left in the dark (black data points). a) A549 cells were cultured in 2D cell monolayers. SRB assay was carried out at t=96 h. The absorbance of Sulforhodamine B in solution was measured at 520 nm. b) A549 cells were cultured as 3D multicellular tumour spheroids in ultra-low attachment flask. The spheroids were treated with [**2**](PF$_6$)$_2$ at day 4, irradiated at day 5 (520 nm, 15 min, 21 mW.cm^{-2}, 19 J.cm^{-2}), and their viability assayed at day 7 by a CellTiter-Glo 3D cell viability assay. Results are presented as means ± SD from three independent experiments with 95% confidence intervals.

Encouraged by these results, the cytotoxicity of [**2**](PF$_6$)$_2$ was further assayed in a wider range of 2D cell monolayer models, i.e. using the PC3Pro4, CRMM1, CRMM2, CM2005.1, OMM1, OMM2.5 and MEL270 human cancer cell lines (Fig. S2). PC3Pro4 is a cancer cell line derived from a bone metastasis obtained after injection of PC3 human prostate cancer cells into nude mice [71], while CRMM1, CRMM2 and CM2005.1 are conjunctival melanoma cell lines and OMM1, OMM2.5 and MEL270 are uveal melanoma cell lines. The EC$_{50}$ values are listed in Table 2 and 3. Interestingly, [**2**](PF$_6$)$_2$ exhibited higher toxicity in PC3Pro4, CRMM1 and CRMM2 cells upon light irradiation, and less toxicity in the dark, resulting in very high PI values of 45, >47, and >59, respectively (Table 3). In order to investigate the cytotoxic mechanism induced by light activated [**2**](PF$_6$)$_2$, CRMM1cells were treated with 4.3 µM for 24 h, stained with Annexin V and propidium iodide, and analysed by fluorescence-activated cell-sorting (FACS). While the fraction of early apoptotic vs. necrotic cells in the cells treated with [**2**](PF$_6$)$_2$ but not irradiated were almost identical to that of the vehicle control, almost half of the cells treated with [**2**](PF$_6$)$_2$ and activated by light were found to be either necrotic (PI+, Annexin–) or in the late apoptotic/dead cell quadrant, while the number of early apoptotic cells decreased to almost zero (Fig. S3). These results come in strong contrast with the almost exclusively apoptotic cell death mode observed with another ruthenium-based PACT compound, [Ru(bapbpy)(dmso)Cl]Cl, showing that the cell death mode with such compounds highly depends on the structure of the complex [72]. Overall, the excellent *in vitro* results observed in PC3Pro4, CRMM1, and CRMM2 cells, led us to selecting these cells for further testing of [**2**](PF$_6$)$_2$ in zebrafish tumour models.

Table 3 Cytotoxicity expressed as effective concentrations (EC_{50} with 95% confidence intervals, in µM) of [**2**]$(PF_6)_2$ in conjunctival melanoma (CRMM1, CRMM2, CM2005.1) and uveal melanoma (OMM1, OMM2.5, MEL270) cell lines, in the dark and upon green light irradiation (21 mW.cm^{-2}, 15 min, 19 J.cm^{-2}, 520 nm).

Cell line	Light dose (J.cm^{-2})	[**2**]$(PF_6)_2$		
		EC_{50}	95%CI	PI
CRMM1	0	>200		
	19	4.3	-0.89 1.1	>47
CRMM2	0	>200		
	19	3.4	-0.88 1.2	>59
CM2005.1	0	>200		
	19	15	-3.2 4.7	>13
OMM1	0	150	-20 30	
	19	24	-4.5 7.6	6.3
OMM2.5	0	100	-8.4 9.2	
	19	14	-1 1.2	7.1
MEL270	0	140	-20 27	
	19	13	-1.3 1.5	11

Maximum tolerated dose of [2]$(PF_6)_2$ in zebrafish ectopic and orthotopic cancer models

To investigate the *in vivo* anti-cancer efficacy of [**2**]$(PF_6)_2$, we utilized prostate (cell line PC3Pro4) and eye (CRMM1, CRMM2, CM2005.1) zebrafish embryonic cancer models, previously established in our group [73,74]. For prostate, androgen-independent osteotropic red-emitting PC3Pro4-mCherry cells (100-400 cells) were intravenously injected into the Duct of Cuvier (DoC) of Tg(Fli:GFP) endothelial reporter transgenic zebrafish line with green fluorescent vasculature (GFP) at 2 days post fertilization (dpf) (Fig. 5). The DoC is an open blood circulation channel connecting the heart and the trunk vasculature of the embryo [75]. Immediately after injection, cells haematogenously disseminated through the whole circulation. Most of the circulating cells regressed without extravasation or initiating tumour growth. However, within 1 day, some cells were able to extravasate exclusively at the posterior ventral end of caudal hematopoietic tissue (CHT), and invade into the tail fin where they developed perivascular metastatic lesions within 4 dpf (Fig. 5). CHT is an intermediate site of haematopoiesis

during zebrafish embryogenesis and is the functional analogue of the foetal liver during mammalian development [76]. Metastatic tumours grew around CHT at 6dpf, as detected by red fluorescence (excitation: 587 nm, emission: 610 nm) that can be quantified, either in terms of emission intensity, or by the relative tumour area in microscopy images; both quantifications are referred below as "relative tumour burden". This tumour model is called "ectopic" as the CHT site does not represent the organ of origin of these cancer cells. For conjunctive melanoma (CM), we used an orthotopic model recently developed in our group for PDT treatment [57,77]. In short, the CM tumours were generated by injection of 200 CRMM1-mCherry or CRMM2-mCherry cells into the retro-orbital site of the embryo at 2 dpf (Fig. 6). From 2 to 6 dpf, the CRMM1 or CRMM2 cells formed local lesions at the injection site behind the eye. This tumour model is called "orthotopic" as the site for tumour growth, i.e. the eye, does represent the organ of origin of these cancer cells.

Table 4 The maximum tolerated dose (MTD) of [**2**]$(PF_6)_2$ in wild type zebrafish embryos and in the ectopic and orthotopic CM tumour models.

[**2**]$(PF_6)_2$	Maximum tolerated concentration	
	Wild Type Embryos	Tumour cells engrafted Embryos Ectopic and Orthotopic Model
Water Administration	1 µM	0.5 µM
Intravenous Administration	300 µM	200 µM
Retro-orbital Administration [a]	300 µM [a]	200 µM [a]

[a] for CRMM1 and CRMM2 xenografts only.

In terms of drug treatment modalities, the embryos were subjected to three different protocols (Fig. 5 and 6). For the ectopic model, treatment with [**2**]$(PF_6)_2$ was performed either by water administration (WA) or by intravenous injection (IV), while for the orthotopic model, treatment was performed either by WA, IV, or retro-orbital (RO) injections. Before testing the anti-tumour efficacy, it was necessary to evaluate the toxicity of the phototherapy treatment. The toxicity of green light alone (520 nm) was recently reported [57]. At an intensity of 21 $mW.cm^{-2}$, the zebrafish embryos could tolerate light irradiation until 6 h without any toxicity or visible developmental defects [57]. The toxicity of [**2**]$(PF_6)_2$ was then evaluated by measuring its maximum tolerated dose (MTD) for the different administration modes, both for tumour-free embryos and tumour cell-injected embryos (Table 4 and Fig. S4). For treatment *via* water administration, different concentrations (0, 0.1 0.25, 0.5, 1, 2 µM) of [**2**]$(PF_6)_2$ were added to the egg water (i.e., the water in which the zebrafish embryo were swimming) at 2.5, 3.5, 4.5 and 5.5 dpf, and incubation was continued overnight for a drug-to-light interval of 12 h. At 3, 4, 5, 6 dpf, excess [**2**]$(PF_6)_2$ was washed by drug-free water and the embryos were further irradiated with green light (21 $mW.cm^{-2}$, 90 min, 114 $J.cm^{-2}$, 520 nm). In such conditions, an MTD of 0.5 µM for embryos engrafted with PC-Pro4-mCherry tumours, and of 1 µM for tumour-cell free embryos, was obtained. For treatment *via* intravenous or retro-orbital administration, 1 nL with different concentrations (0, 50, 100, 200, 300, 500 µM) of [**2**]$(PF_6)_2$ was injected into the dorsal vein or retro-orbital site of zebrafish at 3, 4,

5, 6 dpf. After a shorter drug-light interval of 1 h, the zebrafish embryos were irradiated with the same dose of green light (21 $mW.cm^{-2}$, 90 min, 114 $J.cm^{-2}$, 520 nm). The lethality, aberrant morphology and fish length were measured at 6 dpf. Zebrafish embryos tolerated, without any effect on mortality, malformation and fish length, injection of [**2**]$(PF_6)_2$, followed by light activation, at a MTD of 200 µM for embryos engrafted with PC-Pro4-mCherry, CRMM1, CRMM2 cells and of 300 µM for tumour-free embryos (see Fig. S4). These MTD values of 0.5 µM (WA) and 200 µM (IV and RO) were further used for assessing the anti-tumour efficacy in the zebrafish tumour models.

Effect of [2]$(PF_6)_2$ on PC3Pro4 tumour growth by water and intravenous administration in zebrafish ectopic prostate cancer model

In the PC3Pro4-mCherry zebrafish ectopic model, both WA (0.5 µM) and IV administration (1 nL, 200 µM) of [**2**]$(PF_6)_2$ were tested using the previously determined MTD. At 6 dpf, images of the PC3Pro4-mCherry tumours were taken using a stereo microscope. Quantification of the relative tumour burden was performed by measuring either the relative fluorescence intensity or the relative tumour area (Fig. 5). Using a 12 h (WA) or 1 h (IV) drug-to-light interval, green light activation (21 $mW.cm^{-2}$, 90 min, 114 $J.cm^{-2}$, 520 nm) did not change the tumour burden, compared to the dark groups, even when the treatment on each embryo was repeated 4 times (Fig. 4). Usually, WA in zebrafish is acknowledged to mimic the oral route in human patients. Indeed, the compound will first go into the enterohepatic circulation and then disseminate through the blood circulation. The fact that no anti-tumour activity was observed for [**2**]$(PF_6)_2$ administered by WA in the prostate cancer zebrafish model, while it showed excellent activity in PC3Pro4 cell monolayers *in vitro* (Table 2)*,* suggested that in the embryo, the compound may simply not be taken up into the blood circulation. Another possibility is that it was excreted within the 90 min irradiation time. In contrast, IV injection delivers the compound directly into the blood circulation, but this had no effect either. However, compound [**2**]$(PF_6)_2$ may distribute anywhere in the embryo during the 1 h drug-to-light interval, or be excreted. To obtain anti-tumour efficacy upon light activation requires that the prodrug reaches the tumour in sufficiently high concentrations, which clearly did not happen here. Alternatively, engrafted prostate cancer cells might have gained chemotherapy resistance *in vivo,* which they did not have *in vitro* [78]. Overall, these results most probably suggest that more specific targeting strategies would be needed to achieve proper efficacy of this compound in ectopic prostate cancer models.

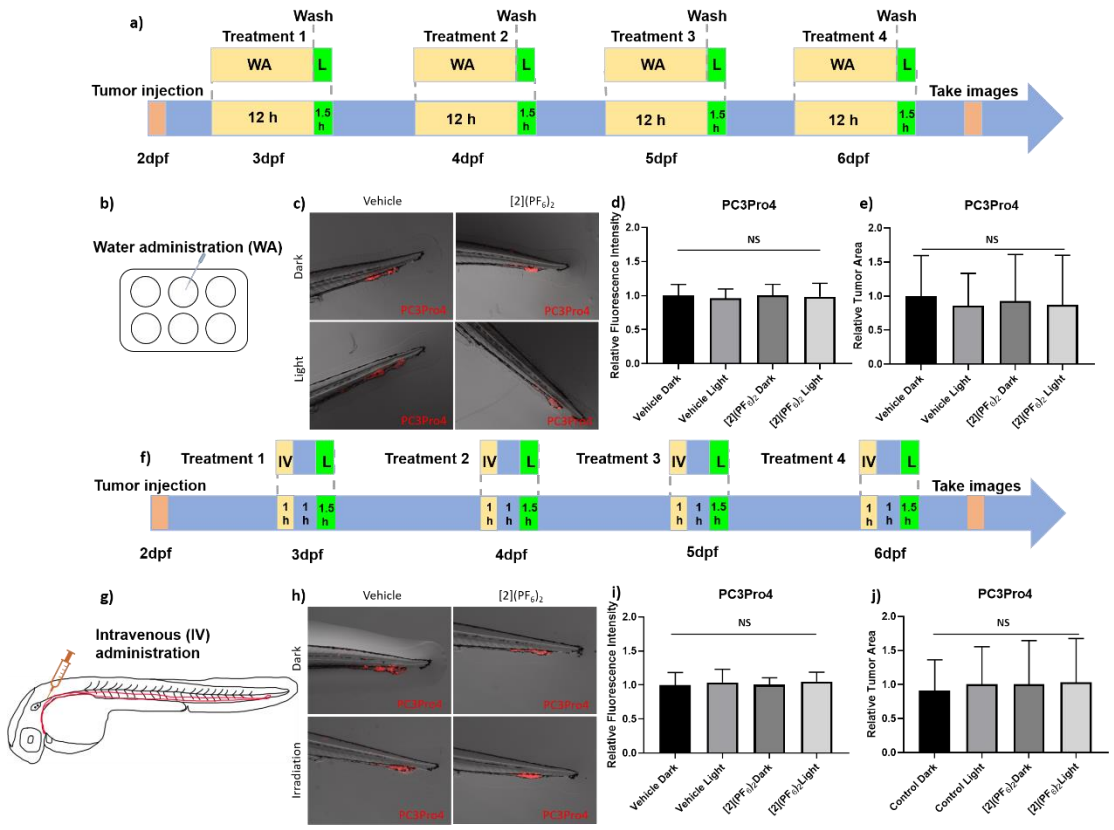

Fig. 5 Efficacy of [**2**]$(PF_6)_2$ in PC3Pro4 prostate cancer zebrafish ectopic model. a) Schedule of tumour cells injection and treatment with [**2**]$(PF_6)_2$ by water administration (WA). Around 300 PC3Pro4 cells were injected into Duct of Cuvier at 2dpf. 0.5 µM of [**2**]$(PF_6)_2$ was added into water at 2.5, 3.5, 4.5, 5.5 dpf. At 3, 4, 5, 6 dpf, the compound was washed away, the embryos were irradiated with green light (21 $mW.cm^{-2}$, 114 $J.cm^{-2}$, 520 nm) for 1.5 h. b) Water administration of [**2**]$(PF_6)_2$ into 6-well plates containing engrafted embryos. c) The images of PC3Pro4 tumour burden at CHT site at 6 dpf. d) The relative fluorescence intensity of PC3Pro4 tumour burden at 6 dpf. e) The relative tumour area of PC3Pro4 tumour burden at 6 dpf) Schedule of tumour cells injections and treatment with 200 µM of [**2**]$(PF_6)_2$ by intravenous administration. g) The injection site of intravenous administration (IV). h) The images of PC3Pro4 tumour burden at CHT site at 6 dpf. i) The relative fluorescence intensity of PC3Pro4 tumour burden at 6 dpf. j) The relative tumour area of PC3Pro4 tumour burden at 6dpf. Results are presented as means ± SD from three independent experiments.

[2](PF$_6$)$_2$ effect on CRMM1 and CRMM2 tumour growth by retro-orbital administration in the zebrafish orthotopic conjunctival melanoma model

When both the tumour cells and the prodrug are injected into the general blood circulation of the embryo, it should not be taken for granted that the drug properly biodistributes to reach the inside of a tumour at a sufficiently high concentration. One way to address this issue is to use a model where the prodrug is injected near the tumour. The efficacy of [**2**]$(PF_6)_2$ was hence examined in the orthotopic model of conjunctival melanoma (CM) described above and in [57]. In this model, the tumour develops

in the back of the eye, near the location of the cancer cell injection, and the prodrug is also injected at the same place. A shorter drug-to-light interval is used (1 h) to avoid prodrug diffusion away from the tumour prior to light activation. In a sense, this model may better mimic local PDT treatments performed in human cancer patients. Following our treatment strategy as developed for the PDT sensitizer TLD-1433 [57], the MTD of [**2**]$(PF_6)_2$ (1 nL, 200 µM) was injected retro-orbitally at 3, 4, 5, 6 dpf. After 1 h drug-to-light interval, the embryos in both light-irradiated groups (vehicle, [**2**]$(PF_6)_2$) were irradiated with green light (520 nm, 90 min, 21 $mW.cm^{-2}$, 114 $J.cm^{-2}$), while the two dark groups (vehicle, [**2**]$(PF_6)_2$) were kept in the dark. During the experiment, the egg water of engrafted embryos was refreshed before injection and after irradiation. At 6 dpf and 4 consecutive treatments, quantification of the CRMM1 and CRMM2 relative tumour burden was performed by measuring either the relative fluorescence intensity or the relative tumour area using a stereo microscope (Fig. 6). In the group treated with [**2**]$(PF_6)_2$ and green light (21 $mW.cm^{-2}$, 114 $J.cm^{-2}$, 520 nm), the CRMM1 tumour burden was significantly inhibited by 57% (fluorescent intensity) and 78% (tumour area) compared with the dark group, while the CRMM2 tumour burden was inhibited by 52% (fluorescence intensity) and 88% (tumour area), compared with the dark group. When comparing these excellent results with the absence of efficacy of the same compound in the ectopic model for prostate cancer, we envision that local RO administration of [**2**]$(PF_6)_2$ generates a higher concentration of the inactive compound in the proximity of the tumour, and therefore that green light activation generates sufficient amounts of the activated ruthenium molecules, to attenuate localized CM development in the light-irradiated group (Fig. 6c-h). These results represent the first experimental demonstration that ruthenium-based PACT treatment can inhibit CM growth in an animal tumour model. They also suggest that compound [**2**]$(PF_6)_2$ should be further investigated in pre-clinical rodent models.

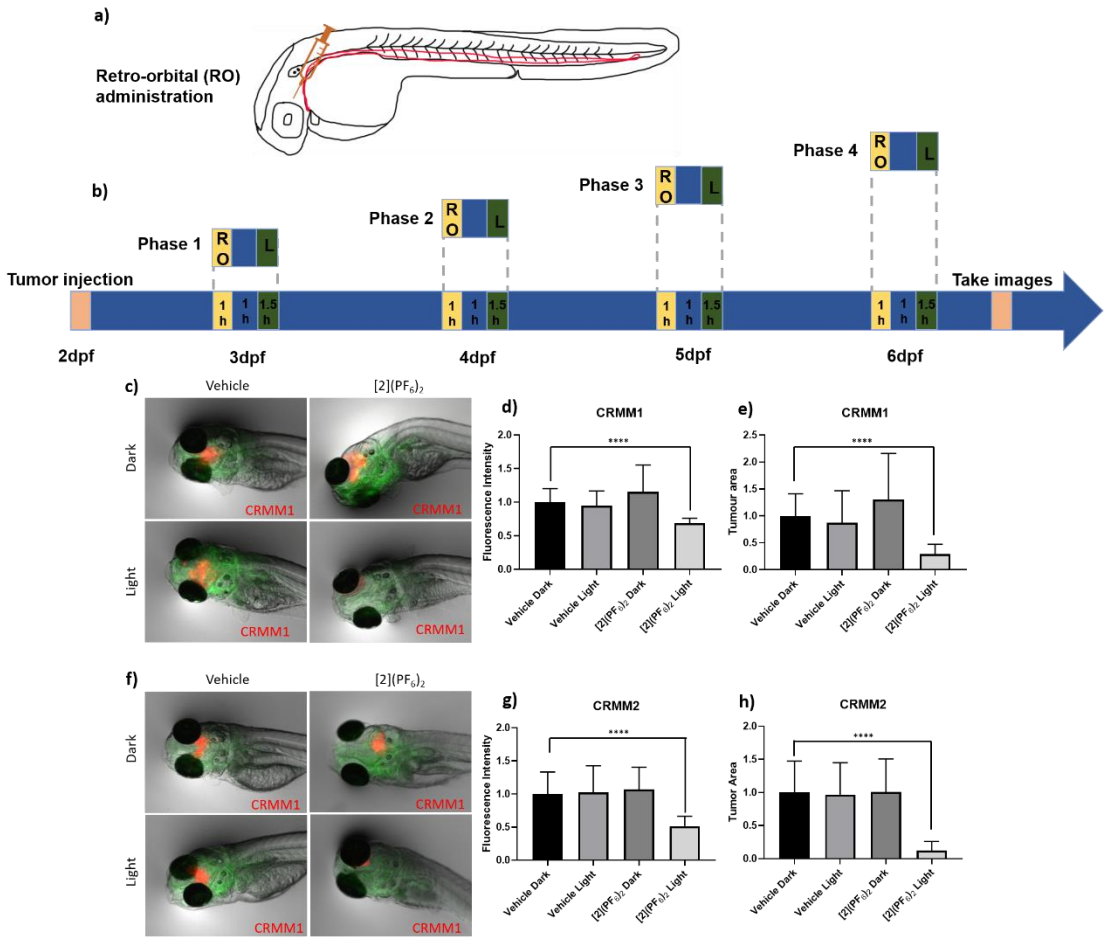

Fig. 6 Efficacy of the PACT compound [**2**](PF$_6$)$_2$ in the Tg(Fli:GFP/casper) zebrafish orthotopic model of conjunctival melanoma (CRMM1 and CRMM2 cell lines) by retro-orbital administration (RO). a) Scheme showing the injection site of retro-orbital administration. b) Time flow of [**2**](PF$_6$)$_2$ treatment with RO administration. Around 200 CRMM1 or CRMM2 cells were injected into the RO site of zebrafish embryos at 2 dpf. [**2**](PF$_6$)$_2$ was injected into RO site at 3, 4, 5, 6 dpf, and after 1 h drug-light interval, the embryos were irradiated with green light (520 nm, 21 mW.cm^{-2}, 90 min, 114 J.cm^{-2}). c) The images of CRMM1 or CRMM2 tumour burden (in red) at CHT site at 6 dpf. Green represents vessels in zebrafish embryos. d, g) The relative red fluorescence (excitation: 554 nm, emission: 581 nm) intensity of CRMM1 or CRMM2 tumour burden at 6 dpf. e, h) The relative tumour area (pixel^2) of CRMM1 or CRMM2 tumour burden at 6dpf. Results are presented as means ± SD from three independent experiments. ****: P < 0.0001.

[2](PF$_6$)$_2$ induces CRMM1 cell apoptosis in the zebrafish orthotopic model

To monitor whether the observed inhibition of CM growth in the zebrafish orthotopic model by [**2**](PF$_6$)$_2$ was occurring *via* apoptosis, an *in situ* TUNEL assay was conducted on fixed embryos bearing CRMM1 tumours at 4 dpi (days post injection), which were either kept in the dark or irradiated with green light (520 nm, 90 min, 21 mW.cm^{-2}, 114 J.cm^{-2}), and treated by RO injection at the MTD (1 nL, 200 µM) either with vehicle control or [**2**](PF$_6$)$_2$ (Fig. 6 and 7). In the TUNNEL assay, the DNA strand breaks in apoptotic tumour cells were stained with fluorescein and visualized as a green signal in microscopy images. In the

dark vehicle group, light vehicle group, and group treated with [**2**]$(PF_6)_2$ but not irradiated, no positive green signal was detected (Fig. 7a). Only in the group treated with [**2**]$(PF_6)_2$ and irradiated with green light (520 nm, 21 $mW.cm^{-2}$, 90 min, 114 $J.cm^{-2}$), a significant number of cancer cells (Fig. 7b) stained positive for apoptotic signal and turned green, which co-localized with red signal of CRMM1 cells (yellow in overlay, Fig. 7a). This result indicated that the anti-tumour efficacy of [**2**]$(PF_6)_2$ in this PACT regime was at least partially apoptosis-dependent, which significantly differs from the FACS analysis *in vitro*. It should also be noted that there was no apoptotic signal detected in the tissue surrounding the tumours, pointing out that light activated [**2**]$(PF_6)_2$ attacked CM tumours but not healthy tissues, which is essential for minimizing side effects.

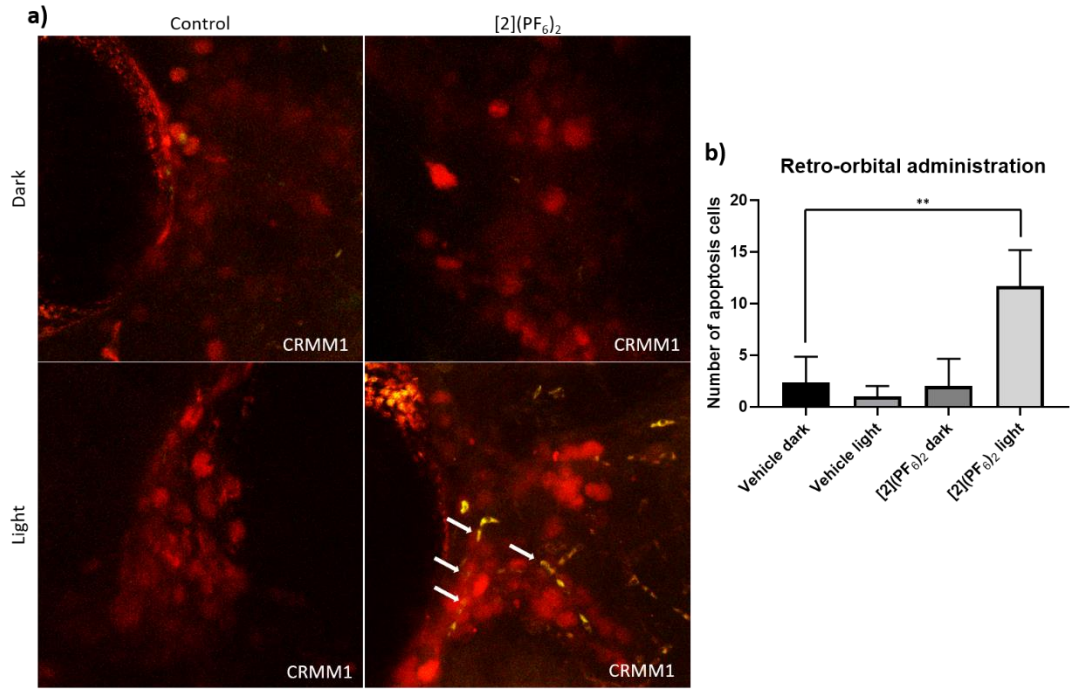

Figure 7 TUNEL assay in the CRMM1 orthotopic tumour model after RO injection of [**2**]$(PF_6)_2$. a) Red fluorescent CRMM1 cells were injected behind the eye of the embryo at 2dpf, and the embryos were divided into four groups for drug treatment. RO administration of vehicle control and [**2**]$(PF_6)_2$ was performed as described in Fig. 6. After dark or light exposure, embryos were fixed and TUNEL staining was performed. a) Representative overlay images of embryos are shown. In the group treated with [**2**]$(PF_6)_2$ and light, nuclear DNA fragmentation in nucleases is detected by co-localization of green (DNA fragments) and red (CM tumour cell) signal, depicted on the overlay as yellow signal marked by white arrows. In the dark control group, light control group, and group treated with [**2**]$(PF_6)_2$ and left in the dark, there were no positive green apoptotic tumour cells. The background green signal in the [**2**]$(PF_6)_2$ light groups did not co-localize with cytosolic red signal, which is diminished in degraded cells and TUNEL stains only the DNA breaks in these CM apoptotic cells. b) Quantification of the number of apoptotic tumour cells (yellow dots). Experiment was performed 3 times with a group size of 10 embryos. **: $P < 0.01$.

Conclusions

In conclusion, we have synthesized the new tris-heteroleptic ruthenium-based PACT prodrug [**2**](PF$_6$)$_2$ which is characterized by a well-balanced hydrophobicity in the dark. The toxicity of this chemical is obtained by green light activation, which triggers photosubstitution of the non-toxic mtmp ligand and liberates a ruthenium-based activated photoproduct. This activated photoproduct can bind to many biomolecules, which ultimately leads to cell death. Of course, [**2**](PF$_6$)$_2$ has not been designed for specific targets in tumour cells, which may be seen as a potential sources of side-effects. On the other hand, this lack of specificity ensures that single mutations in cancer cells would not quench the cytotoxic activity of the light-activated compound, as confirmed by the large range of unrelated cancer cell lines (lung, prostate, eye) in which [**2**](PF$_6$)$_2$ remained photoactive. Still, differences in photoindexes existed between cell lines, which pointed at PC3Pro4, CRMM1, and CRMM2 cell lines, for further *in vivo* evaluation. We do not know why the uveal melanoma cell lines did not show a better response to the treatment with [**2**](PF$_6$)$_2$, but we decided to use the conjunctival cell lines when we saw how much more sensitive these were. Zebrafish embryos allowed us to demonstrate the efficacy of ruthenium-based PACT in conjunctival melanoma xenografts *in vivo* [48]; this provided the first MTD values for a photosubstitutionally active ruthenium compound administered either *via* water, intravenous injection, or retro-orbital injection. More than this, our results also highlight the difference between ectopic and orthotopic *in vivo* models for photoactivated drugs: while the photoindexes *in vitro* were high both in prostate cancer cells (PC3Pro4) and conjunctival melanoma cells (CRMM1, CRMM2), *in vivo* there was no activity in the ectopic model of prostate cancer, while activity was excellent in the orthotopic model of conjunctival melanoma. Such a difference underscores the interaction between the type of tumour model as well as the mode of compound administration in tumour xenografts, which cannot be modelled *in vitro* but dramatically influence both (pro)drug biodistribution, drug uptake by the tumour, and hence the final anti-tumour efficacy of the treatment. Overall, the present validation of the anti-tumour efficacy of retro-orbitally administered ruthenium compound [**2**](PF$_6$)$_2$ in zebrafish conjunctival melanoma orthotopic models suggests that further pre-clinical development of this new PACT drug should be considered in larger models (rodents) for conjunctival melanoma, where light irradiation can be limited to the tumour.

Conflict of interest

There are no conflicts of interest to declare.

Acknowledgements

The European Research Council is kindly acknowledged for a Starting Grant (RuProLight) and a Proof-of-Concept grant (Ru4EYE) to S.B. The Chinese Scholarship Council is kindly acknowledged for a PhD grants to Q.C.

References

1. Dilruba, S.; Kalayda, G.V. Platinum-based drugs: past, present and future. *Cancer chemotherapy and pharmacology* **2016**, *77*, 1103-1124, doi:10.1007/s00280-016-2976-z.
2. Galanski, M. Recent developments in the field of anticancer platinum complexes. *Recent patents on anti-cancer drug discovery* **2006**, *1*, 285-295, doi:10.2174/157489206777442287.
3. Lebwohl, D.; Canetta, R. Clinical development of platinum complexes in cancer therapy: an historical perspective and an update. *European journal of cancer (Oxford, England : 1990)* **1998**, *34*, 1522-1534, doi:10.1016/s0959-8049(98)00224-x.
4. Pouysségur, J.; Dayan, F.; Mazure, N.M. Hypoxia signalling in cancer and approaches to enforce tumour regression. *Nature* **2006**, *441*, 437-443, doi:10.1038/nature04871.
5. Jamieson, E.R.; Lippard, S.J. Structure, Recognition, and Processing of Cisplatin-DNA Adducts. *Chemical reviews* **1999**, *99*, 2467-2498, doi:10.1021/cr980421n.
6. Fraval, H.N.; Rawlings, C.J.; Roberts, J.J. Increased sensitivity of UV-repair-deficient human cells to DNA bound platinum products which unlike thymine dimers are not recognized by an endonuclease extracted from Micrococcus luteus. *Mutation research* **1978**, *51*, 121-132, doi:10.1016/0027-5107(78)90014-3.
7. Dasari, S.; Tchounwou, P.B. Cisplatin in cancer therapy: molecular mechanisms of action. *European journal of pharmacology* **2014**, *740*, 364-378, doi:10.1016/j.ejphar.2014.07.025.
8. Karasawa, T.; Steyger, P.S. An integrated view of cisplatin-induced nephrotoxicity and ototoxicity. *Toxicology letters* **2015**, *237*, 219-227, doi:10.1016/j.toxlet.2015.06.012.
9. Cersosimo, R.J. Hepatotoxicity associated with cisplatin chemotherapy. *The Annals of pharmacotherapy* **1993**, *27*, 438-441, doi:10.1177/106002809302700408.
10. Martins, N.M.; Santos, N.A.; Curti, C.; Bianchi, M.L.; Santos, A.C. Cisplatin induces mitochondrial oxidative stress with resultant energetic metabolism impairment, membrane rigidification and apoptosis in rat liver. *Journal of applied toxicology : JAT* **2008**, *28*, 337-344, doi:10.1002/jat.1284.
11. Kenny, R.G.; Marmion, C.J. Toward Multi-Targeted Platinum and Ruthenium Drugs-A New Paradigm in Cancer Drug Treatment Regimens? *Chemical reviews* **2019**, *119*, 1058-1137, doi:10.1021/acs.chemrev.8b00271.
12. Garner, R.N.; Gallucci, J.C.; Dunbar, K.R.; Turro, C. [Ru(bpy)2(5-cyanouracil)2]2+ as a potential light-activated dual-action therapeutic agent. *Inorganic chemistry* **2011**, *50*, 9213-9215, doi:10.1021/ic201615u.
13. Respondek, T.; Garner, R.N.; Herroon, M.K.; Podgorski, I.; Turro, C.; Kodanko, J.J. Light activation of a cysteine protease inhibitor: caging of a peptidomimetic nitrile with Ru(II)(bpy)2. *Journal of the American Chemical Society* **2011**, *133*, 17164-17167, doi:10.1021/ja208084s.
14. Cuello-Garibo, J.-A.; Meijer, M.S.; Bonnet, S. To cage or to be caged? The cytotoxic species in ruthenium-based photoactivated chemotherapy is not always the metal. *Chem Commun (Camb)* **2017**, *53*, 6768-6771, doi:10.1039/c7cc03469e.
15. Wilson, W.R.; Hay, M.P. Targeting hypoxia in cancer therapy. *Nat Rev Cancer* **2011**, *11*, 393-410, doi:10.1038/nrc3064.
16. Lameijer, L.N.; Ernst, D.; Hopkins, S.L.; Meijer, M.S.; Askes, S.H.C.; Le Dévédec, S.E.; Bonnet, S. A Red-Light-Activated Ruthenium-Caged NAMPT Inhibitor Remains Phototoxic in Hypoxic Cancer Cells. *Angew Chem Int Ed Engl* **2017**, *56*, 11549-11553, doi:10.1002/anie.201703890.
17. Bonnet, S. Why develop photoactivated chemotherapy? *Dalton transactions (Cambridge, England : 2003)* **2018**, *47*, 10330-10343, doi:10.1039/c8dt01585f.
18. Mari, C.; Gasser, G. Lightening up Ruthenium Complexes to Fight Cancer? *Chimia (Aarau)* **2015**, *69*, 176-181, doi:10.2533/chimia.2015.176.
19. Farrer, N.J.; Salassa, L.; Sadler, P.J. Photoactivated chemotherapy (PACT): the potential of excited-state d-block metals in medicine. *Dalton transactions (Cambridge, England : 2003)* **2009**, 10.1039/b917753a, 10690-10701, doi:10.1039/b917753a.
20. Arora, K.; Herroon, M.; Al-Afyouni, M.H.; Toupin, N.P.; Rohrabaugh, T.N., Jr.; Loftus, L.M.; Podgorski, I.; Turro, C.; Kodanko, J.J. Catch and Release Photosensitizers: Combining Dual-Action Ruthenium Complexes with Protease Inactivation for Targeting Invasive Cancers. *Journal of the American Chemical Society* **2018**, *140*, 14367-14380,

doi:10.1021/jacs.8b08853.
21. Zhou, Q.-X.; Lei, W.-H.; Chen, J.-R.; Li, C.; Hou, Y.-J.; Wang, X.-S.; Zhang, B.-W. A new heteroleptic ruthenium(II) polypyridyl complex with long-wavelength absorption and high singlet-oxygen quantum yield. *Chemistry* **2010**, *16*, 3157-3165, doi:10.1002/chem.200902563.
22. Sainuddin, T.; Pinto, M.; Yin, H.; Hetu, M.; Colpitts, J.; McFarland, S.A. Strained ruthenium metal–organic dyads as photocisplatin agents with dual action. *Journal of Inorganic Biochemistry* **2016**, *158*, 45-54, doi:https://doi.org/10.1016/j.jinorgbio.2016.01.009.
23. Hufziger, K.T.; Thowfeik, F.S.; Charboneau, D.J.; Nieto, I.; Dougherty, W.G.; Kassel, W.S.; Dudley, T.J.; Merino, E.J.; Papish, E.T.; Paul, J.J. Ruthenium dihydroxybipyridine complexes are tumor activated prodrugs due to low pH and blue light induced ligand release. *Journal of Inorganic Biochemistry* **2014**, *130*, 103-111, doi:http://dx.doi.org/10.1016/j.jinorgbio.2013.10.008.
24. Howerton, B.S.; Heidary, D.K.; Glazer, E.C. Strained ruthenium complexes are potent light-activated anticancer agents. *Journal of the American Chemical Society* **2012**, *134*, 8324-8327, doi:10.1021/ja3009677.
25. Meijer, M.S.; Bonnet, S. Diastereoselective Synthesis and Two-Step Photocleavage of Ruthenium Polypyridyl Complexes Bearing a Bis(thioether) Ligand. *Inorganic chemistry* **2019**, *58*, 11689-11698, doi:10.1021/acs.inorgchem.9b01669.
26. Wachter, E.; Heidary, D.K.; Howerton, B.S.; Parkin, S.; Glazer, E.C. Light-activated ruthenium complexes photobind DNA and are cytotoxic in the photodynamic therapy window. *Chem Commun (Camb)* **2012**, *48*, 9649-9651, doi:10.1039/c2cc33359g.
27. Roque, J., 3rd; Havrylyuk, D.; Barrett, P.C.; Sainuddin, T.; McCain, J.; Colón, K.; Sparks, W.T.; Bradner, E.; Monro, S.; Heidary, D., et al. Strained, Photoejecting Ru(II) Complexes that are Cytotoxic Under Hypoxic Conditions. *Photochemistry and photobiology* **2020**, *96*, 327-339, doi:10.1111/php.13174.
28. Albani, B.A.; Peña, B.; Dunbar, K.R.; Turro, C. New cyclometallated Ru(II) complex for potential application in photochemotherapy? *Photochemical & photobiological sciences : Official journal of the European Photochemistry Association and the European Society for Photobiology* **2014**, *13*, 272-280, doi:10.1039/c3pp50327e.
29. Hufziger, K.T.; Thowfeik, F.S.; Charboneau, D.J.; Nieto, I.; Dougherty, W.G.; Kassel, W.S.; Dudley, T.J.; Merino, E.J.; Papish, E.T.; Paul, J.J. Ruthenium dihydroxybipyridine complexes are tumor activated prodrugs due to low pH and blue light induced ligand release. *Journal of inorganic biochemistry* **2014**, *130*, 103-111, doi:10.1016/j.jinorgbio.2013.10.008.
30. Letrado, P.; de Miguel, I.; Lamberto, I.; Díez-Martínez, R.; Oyarzabal, J. Zebrafish: Speeding Up the Cancer Drug Discovery Process. *Cancer Res* **2018**, *78*, 6048-6058, doi:10.1158/0008-5472.CAN-18-1029.
31. Kucinska, M.; Murias, M.; Nowak-Sliwinska, P. Beyond mouse cancer models: Three-dimensional human-relevant in vitro and non-mammalian in vivo models for photodynamic therapy. *Mutation research* **2017**, *773*, 242-262, doi:10.1016/j.mrrev.2016.09.002.
32. Letrado, P.; de Miguel, I.; Lamberto, I.; Díez-Martínez, R.; Oyarzabal, J. Zebrafish: Speeding Up the Cancer Drug Discovery Process. *Cancer Res* **2018**, *78*, 6048-6058, doi:10.1158/0008-5472.can-18-1029.
33. Xiao, J.; Glasgow, E.; Agarwal, S. Zebrafish Xenografts for Drug Discovery and Personalized Medicine. *Trends in cancer* **2020**, 10.1016/j.trecan.2020.03.012, doi:10.1016/j.trecan.2020.03.012.
34. Amatruda, J.F.; Shepard, J.L.; Stern, H.M.; Zon, L.I. Zebrafish as a cancer model system. *Cancer Cell* **2002**, *1*, 229-231, doi:10.1016/s1535-6108(02)00052-1.
35. Zhang, X.; de Boer, L.; Heiliegers, L.; Man-Bovenkerk, S.; Selbo, P.K.; Drijfhout, J.W.; Høgset, A.; Zaat, S.A.J. Photochemical internalization enhances cytosolic release of antibiotic and increases its efficacy against staphylococcal infection. *Journal of controlled release : official journal of the Controlled Release Society* **2018**, *283*, 214-222, doi:10.1016/j.jconrel.2018.06.004.
36. Mauriello Jimenez, C.; Aggad, D.; Croissant, J.G.; Tresfield, K.; Laurencin, D.; Berthomieu, D.; Cubedo, N.; Rossel, M.; Alsaiari, S.; Anjum, D.H., et al. Porous Porphyrin-Based Organosilica Nanoparticles for NIR Two-Photon Photodynamic Therapy and Gene Delivery in Zebrafish. *Advanced Functional Materials* **2018**, *28*, 1800235, doi:10.1002/adfm.201800235.

37. Matera, C.; Gomila, A.M.J.; Camarero, N.; Libergoli, M.; Soler, C.; Gorostiza, P. Photoswitchable Antimetabolite for Targeted Photoactivated Chemotherapy. *Journal of the American Chemical Society* **2018**, *140*, 15764-15773, doi:10.1021/jacs.8b08249.
38. Bouchaala, R.; Anton, N.; Anton, H.; Vandamme, T.; Vermot, J.; Smail, D.; Mély, Y.; Klymchenko, A.S. Light-triggered release from dye-loaded fluorescent lipid nanocarriers in vitro and in vivo. *Colloids and surfaces. B, Biointerfaces* **2017**, *156*, 414-421, doi:10.1016/j.colsurfb.2017.05.035.
39. He, J.; Wang, Y.; Missinato, M.A.; Onuoha, E.; Perkins, L.A.; Watkins, S.C.; St Croix, C.M.; Tsang, M.; Bruchez, M.P. A genetically targetable near-infrared photosensitizer. *Nature methods* **2016**, *13*, 263-268, doi:10.1038/nmeth.3735.
40. Li, S.P.; Lau, C.T.; Louie, M.W.; Lam, Y.W.; Cheng, S.H.; Lo, K.K. Mitochondria-targeting cyclometalated iridium(III)-PEG complexes with tunable photodynamic activity. *Biomaterials* **2013**, *34*, 7519-7532, doi:10.1016/j.biomaterials.2013.06.028.
41. Manghnani, P.N.; Wu, W.; Xu, S.; Hu, F.; Teh, C.; Liu, B. Visualizing Photodynamic Therapy in Transgenic Zebrafish Using Organic Nanoparticles with Aggregation-Induced Emission. *Nano-micro letters* **2018**, *10*, 61, doi:10.1007/s40820-018-0214-4.
42. Bai, C.; Tang, M. Toxicological study of metal and metal oxide nanoparticles in zebrafish. *Journal of applied toxicology : JAT* **2020**, *40*, 37-63, doi:10.1002/jat.3910.
43. Wehmas, L.C.; Anders, C.; Chess, J.; Punnoose, A.; Pereira, C.B.; Greenwood, J.A.; Tanguay, R.L. Comparative Metal Oxide Nanoparticle Toxicity Using Embryonic Zebrafish. *Toxicology reports* **2015**, *2*, 702-715, doi:10.1016/j.toxrep.2015.03.015.
44. Gutiérrez-Lovera, C.; Martínez-Val, J.; Cabezas-Sainz, P.; López, R.; Rubiolo, J.A.; Sánchez, L. In vivo toxicity assays in zebrafish embryos: a pre-requisite for xenograft preclinical studies. *Toxicology mechanisms and methods* **2019**, *29*, 478-487, doi:10.1080/15376516.2019.1611980.
45. Das, B.C.; McCormick, L.; Thapa, P.; Karki, R.; Evans, T. Use of zebrafish in chemical biology and drug discovery. *Future medicinal chemistry* **2013**, *5*, 2103-2116, doi:10.4155/fmc.13.170.
46. Zon, L.I.; Peterson, R.T. In vivo drug discovery in the zebrafish. *Nature reviews. Drug discovery* **2005**, *4*, 35-44, doi:10.1038/nrd1606.
47. Cuello-Garibo, J.A.; Meijer, M.S.; Bonnet, S. To cage or to be caged? The cytotoxic species in ruthenium-based photoactivated chemotherapy is not always the metal. *Chem Commun (Camb)* **2017**, *53*, 6768-6771, doi:10.1039/c7cc03469e.
48. Reisner, E.; Abikoff, T.C.; Lippard, S.J. Influence of steric hindrance on the core geometry and sulfoxidation chemistry of carboxylate-rich diiron(II) complexes. *Inorganic chemistry* **2007**, *46*, 10229-10240, doi:10.1021/ic7014176.
49. Bahreman, A.; Cuello-Garibo, J.A.; Bonnet, S. Yellow-light sensitization of a ligand photosubstitution reaction in a ruthenium polypyridyl complex covalently bound to a rhodamine dye. *Dalton transactions (Cambridge, England : 2003)* **2014**, *43*, 4494-4505, doi:10.1039/c3dt52643g.
50. Nareyeck, G.; Wuestemeyer, H.; von der Haar, D.; Anastassiou, G. Establishment of two cell lines derived from conjunctival melanomas. *Experimental eye research* **2005**, *81*, 361-362, doi:10.1016/j.exer.2005.04.018.
51. Keijser, S.; Maat, W.; Missotten, G.S.; de Keizer, R.J. A new cell line from a recurrent conjunctival melanoma. *The British journal of ophthalmology* **2007**, *91*, 1566-1567, doi:10.1136/bjo.2006.110841.
52. Luyten, G.P.; Naus, N.C.; Mooy, C.M.; Hagemeijer, A.; Kan-Mitchell, J.; Van Drunen, E.; Vuzevski, V.; De Jong, P.T.; Luider, T.M. Establishment and characterization of primary and metastatic uveal melanoma cell lines. *International journal of cancer* **1996**, *66*, 380-387, doi:10.1002/(sici)1097-0215(19960503)66:3<380::aid-ijc19>3.0.co;2-f.
53. Chen, P.W.; Murray, T.G.; Uno, T.; Salgaller, M.L.; Reddy, R.; Ksander, B.R. Expression of MAGE genes in ocular melanoma during progression from primary to metastatic disease. *Clinical & experimental metastasis* **1997**, *15*, 509-518, doi:10.1023/a:1018479011340.
54. Carlotti, F.; Bazuine, M.; Kekarainen, T.; Seppen, J.; Pognonec, P.; Maassen, J.A.; Hoeben, R.C. Lentiviral vectors efficiently transduce quiescent mature 3T3-L1 adipocytes. *Molecular therapy : the journal of the American Society of Gene Therapy* **2004**, *9*, 209-217, doi:10.1016/j.ymthe.2003.11.021.

55. Schatzschneider, U.; Niesel, J.; Ott, I.; Gust, R.; Alborzinia, H.; Wölfl, S. Cellular Uptake, Cytotoxicity, and Metabolic Profiling of Human Cancer Cells Treated with Ruthenium(II) Polypyridyl Complexes [Ru(bpy)2(N N)]Cl2 with N N=bpy, phen, dpq, dppz, and dppn. *ChemMedChem* **2008**, *3*, 1104-1109, doi:10.1002/cmdc.200800039.
56. Hopkins, S.L.; Siewert, B.; Askes, S.H.; Veldhuizen, P.; Zwier, R.; Heger, M.; Bonnet, S. An in vitro cell irradiation protocol for testing photopharmaceuticals and the effect of blue, green, and red light on human cancer cell lines. *Photochemical & photobiological sciences : Official journal of the European Photochemistry Association and the European Society for Photobiology* **2016**, *15*, 644-653, doi:10.1039/c5pp00424a.
57. Chen, Q.; Ramu, V.; Aydar, Y.; Groenewoud, A.; Zhou, X.Q.; Jager, M.J.; Cole, H.; Cameron, C.G.; McFarland, S.A.; Bonnet, S., et al. TLD1433 Photosensitizer Inhibits Conjunctival Melanoma Cells in Zebrafish Ectopic and Orthotopic Tumour Models. *Cancers* **2020**, *12*, doi:10.3390/cancers12030587.
58. Lawson, N.D.; Weinstein, B.M. In vivo imaging of embryonic vascular development using transgenic zebrafish. *Dev Biol* **2002**, *248*, 307-318, doi:10.1006/dbio.2002.0711.
59. Burke, C.S.; Keyes, T.E. An efficient route to asymmetrically diconjugated tris(heteroleptic) complexes of Ru(ii). *RSC Advances* **2016**, *6*, 40869-40877, doi:10.1039/C6RA06086B.
60. Mari, C.; Pierroz, V.; Rubbiani, R.; Patra, M.; Hess, J.; Spingler, B.; Oehninger, L.; Schur, J.; Ott, I.; Salassa, L., et al. DNA Intercalating Ru-II Polypyridyl Complexes as Effective Photosensitizers in Photodynamic Therapy. *Chemistry-a European Journal* **2014**, *20*, 14421-14436, doi:10.1002/chem.201402796.
61. Frei, A.; Rubbiani, R.; Tubafard, S.; Blacque, O.; Anstaett, P.; Felgentrager, A.; Maisch, T.; Spiccia, L.; Gasser, G. Synthesis, Characterization, and Biological Evaluation of New Ru(II) Polypyridyl Photosensitizers for Photodynamic Therapy. *Journal of Medicinal Chemistry* **2014**, *57*, 7280-7292, doi:10.1021/jm500566f.
62. Shi, G.; Monro, S.; Hennigar, R.; Colpitts, J.; Fong, J.; Kasimova, K.; Yin, H.; DeCoste, R.; Spencer, C.; Chamberlain, L., et al. Ru(II) dyads derived from α-oligothiophenes: A new class of potent and versatile photosensitizers for PDT. *Coordination Chemistry Reviews* **2015**, *282–283*, 127-138, doi:http://dx.doi.org/10.1016/j.ccr.2014.04.012.
63. Garcìa-Fresnadillo, D.; Georgiadou, Y.; Orellana, G.; Braun, A.M.; Oliveros, E. Singlet-Oxygen (1Δg) Production by Ruthenium(II) complexes containing polyazaheterocyclic ligands in methanol and in water. *Helvetica Chimica Acta* **1996**, *79*, 1222-1238, doi:10.1002/hlca.19960790428.
64. Moan, J.; Sommer, S. Oxygen dependence of the photosensitizing effect of hematoporphyrin derivative in NHIK 3025 cells. *Cancer Res* **1985**, *45*, 1608-1610.
65. Bonnett, R. *Studies on 5,10,15,20-tetrakis(m-hydroxyphenyl)chlorin, mTHPC (Temoporfin)*; SPIE: 1995; Vol. 2371.
66. Arenas, Y.; Monro, S.; Shi, G.; Mandel, A.; McFarland, S.; Lilge, L. Photodynamic inactivation of Staphylococcus aureus and methicillin-resistant Staphylococcus aureus with Ru(II)-based type I/type II photosensitizers. *Photodiagnosis and photodynamic therapy* **2013**, *10*, 615-625, doi:10.1016/j.pdpdt.2013.07.001.
67. Hopkins, S.L.; Siewert, B.; Askes, S.H.C.; Veldhuizen, P.; Zwier, R.; Heger, M.; Bonnet, S. An in vitro cell irradiation protocol for testing photopharmaceuticals and the effect of blue, green, and red light on human cancer cell lines. *Photochemical & Photobiological Sciences* **2016**, *15*, 644-653, doi:10.1039/C5PP00424A.
68. Lameijer, L.N.; Ernst, D.; Hopkins, S.L.; Meijer, M.S.; Askes, S.H.C.; Le Dévédec, S.E.; Bonnet, S. A Red-Light-Activated Ruthenium-Caged NAMPT Inhibitor Remains Phototoxic in Hypoxic Cancer Cells. *Angewandte Chemie International Edition* **2017**, *56*, 11549-11553, doi:10.1002/anie.201703890.
69. Horobin, R.W.; Stockert, J.C.; Rashid-Doubell, F. Fluorescent cationic probes for nuclei of living cells: why are they selective? A quantitative structure–activity relations analysis. *Histochemistry and Cell Biology* **2006**, *126*, 165-175, doi:10.1007/s00418-006-0156-7.
70. Puckett, C.A.; Barton, J.K. Methods to Explore Cellular Uptake of Ruthenium Complexes. *Journal of the American Chemical Society* **2007**, *129*, 46-47, doi:10.1021/ja0677564.
71. Pettaway, C.A.; Pathak, S.; Greene, G.; Ramirez, E.; Wilson, M.R.; Killion, J.J.; Fidler, I.J. Selection of highly metastatic variants of different human prostatic carcinomas using orthotopic implantation in nude mice. *Clinical Cancer Research* **1996**, *2*, 1627-1636.

72. van Rixel, V.H.S.; Siewert, B.; Hopkins, S.L.; Askes, S.H.C.; Busemann, A.; Siegler, M.A.; Bonnet, S. Green light-induced apoptosis in cancer cells by a tetrapyridyl ruthenium prodrug offering two trans coordination sites. *Chemical science* **2016**, *7*, 4922-4929, doi:10.1039/c6sc00167j.
73. Hill, D.; Chen, L.; Snaar-Jagalska, E.; Chaudhry, B. Embryonic zebrafish xenograft assay of human cancer metastasis. *F1000Research* **2018**, *7*, 1682, doi:10.12688/f1000research.16659.2.
74. van der Ent, W.; Burrello, C.; Teunisse, A.F.; Ksander, B.R.; van der Velden, P.A.; Jager, M.J.; Jochemsen, A.G.; Snaar-Jagalska, B.E. Modeling of human uveal melanoma in zebrafish xenograft embryos. *Investigative ophthalmology & visual science* **2014**, *55*, 6612-6622, doi:10.1167/iovs.14-15202.
75. Drabsch, Y.; He, S.; Zhang, L.; Snaar-Jagalska, B.E.; ten Dijke, P. Transforming growth factor-β signalling controls human breast cancer metastasis in a zebrafish xenograft model. *Breast Cancer Res* **2013**, *15*, R106-R106, doi:10.1186/bcr3573.
76. Murayama, E.; Kissa, K.; Zapata, A.; Mordelet, E.; Briolat, V.; Lin, H.-F.; Handin, R.I.; Herbomel, P. Tracing hematopoietic precursor migration to successive hematopoietic organs during zebrafish development. *Immunity* **2006**, *25*, 963-975, doi:10.1016/j.immuni.2006.10.015.
77. Monro, S.; Colón, K.L.; Yin, H.; Roque, J., 3rd; Konda, P.; Gujar, S.; Thummel, R.P.; Lilge, L.; Cameron, C.G.; McFarland, S.A. Transition Metal Complexes and Photodynamic Therapy from a Tumor-Centered Approach: Challenges, Opportunities, and Highlights from the Development of TLD1433. *Chemical reviews* **2019**, *119*, 797-828, doi:10.1021/acs.chemrev.8b00211.
78. Wang, G.; Zhao, D.; Spring, D.J.; DePinho, R.A. Genetics and biology of prostate cancer. *Genes Dev* **2018**, *32*, 1105-1140, doi:10.1101/gad.315739.118.

Supporting information for

Photosubstitution in a new trisheteroleptic ruthenium complex inhibits conjunctival melanoma growth in zebrafish orthotopic xenograft model

Quanchi Chen [1#], Jordi-Amat Cuello-Garibo [2#], Vadde Ramu [2], Yasmin Aydar [1], Yevhen Batsuin,[2] Sharon Bronkhorst [2], Nataliia Beztsinna [2], Lanpeng Chen [1], Xue-Quan Zhou [2], Claudia Schmidt [3], Ingo Ott [3], Martine J. Jager [4], B. Ewa Snaar-Jagalska [1*], Sylvestre Bonnet [2*]

[1] Institute of Biology, Leiden University, Leiden, The Netherlands
[2] Leiden Institute of Chemistry, Leiden University, P.O. Box 9502, 2300 RA Leiden, The Netherlands
[3] Institute of Medicinal and Pharmaceutical Chemistry, Technische Universität Braunschweig, Beethovenstrasse 55, D-38106 Braunschweig, Germany
[4] Department of Ophthalmology, Leiden University Medical Center, Leiden, The Netherlands
# These authors contributed equally to the paper
* Correspondence: b.e.snaar-jagalska@biology.leidenuniv.nl ; Tel.: +31-71-527-4980 (E.S.J.); bonnet@chem.leidenuniv.nl ; Tel : +31-71-527-4260 (S.B.);

QUANTUM YIELD DETERMINATION

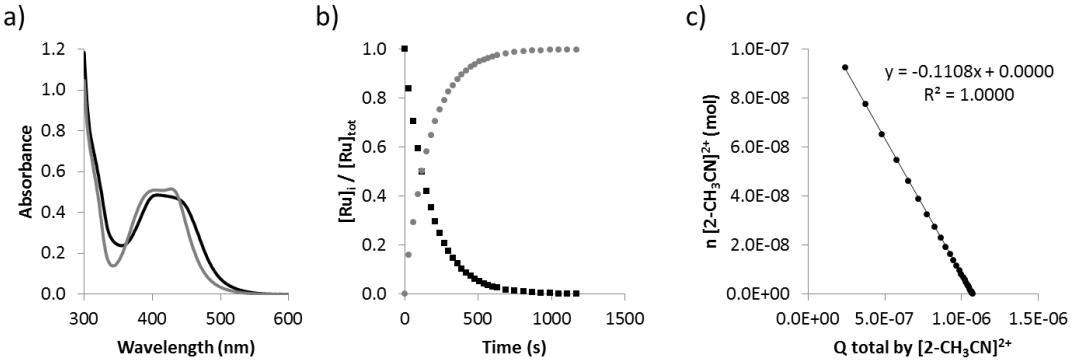

Figure S1 Kinetic data for the second step of the photosubstitution of [**2**]$(PF_6)_2$ in CH_3CN under N_2. a) Globally fitted absorption spectra of the mono-aqua intermediate [Ru(dpp)(bpy)(η^1-mtmp)(CH_3CN)] ([**2**-CH_3CN] , black) and $[Ru(dpp)_2(CH_3CN)_2]^{2+}$ (grey) according to modeling using the Glotaran software. b) Modeled evolution of the relative concentrations of [**2**- $CH_3CN]^{2+}$ (squares) and $[Ru(dpp)_2(CH_3CN)_2]^{2+}$ (circles) vs. irradiation time according to global fitting using Glotaran. c) Plot of the amount of [**2**-$CH_3CN]^{2+}$ (mol) vs. total amount of photons absorbed by [**2**-$CH_3CN]^{2+}$ (mol). The slope of the obtained line is the opposite of the quantum yield of the formation of the bis-aqua complex. Conditions: 0.036 mM solution of [**2**]$(PF_6)_2$ in CH_3CN irradiated at 298 K under N_2 using a 521 nm LED at $6.21 \cdot 10^{-8}$ mol·s^{-1}.

DOSE-RESPONSE CURVES IN CONJUNCTIVE MELANOMA, UVEAL MELANOMA AND PROSTATE CANCER CELL LINES

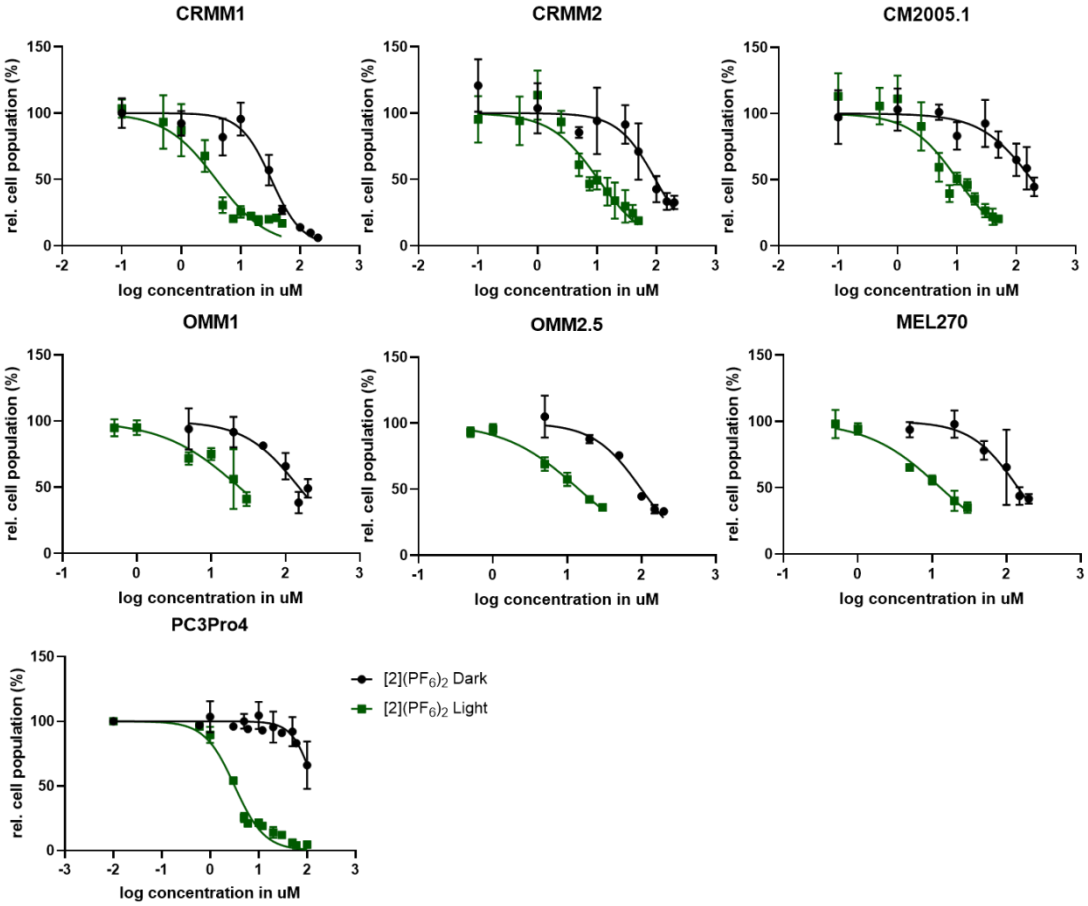

Figure S2 Dose-response curves for CRMM1, CRMM2, CM2005.1, OMM1, OMM2.5, MEL270 and PC3Pro4 cells treated with [**2**]$(PF_6)_2$ and irradiated with green light (520 nm, 21 mW/cm^2, 19 J.cm^{-2}) 24 h after treatment (green data points) or left in the dark (black data points). SRB assay was carried out at t=96 h. The absorbance of Sulforhodamine B in solution was measured at 520 nm. Results are presented as means ± SD from three independent experiments.

ANNEXIN V-PI ASSAY

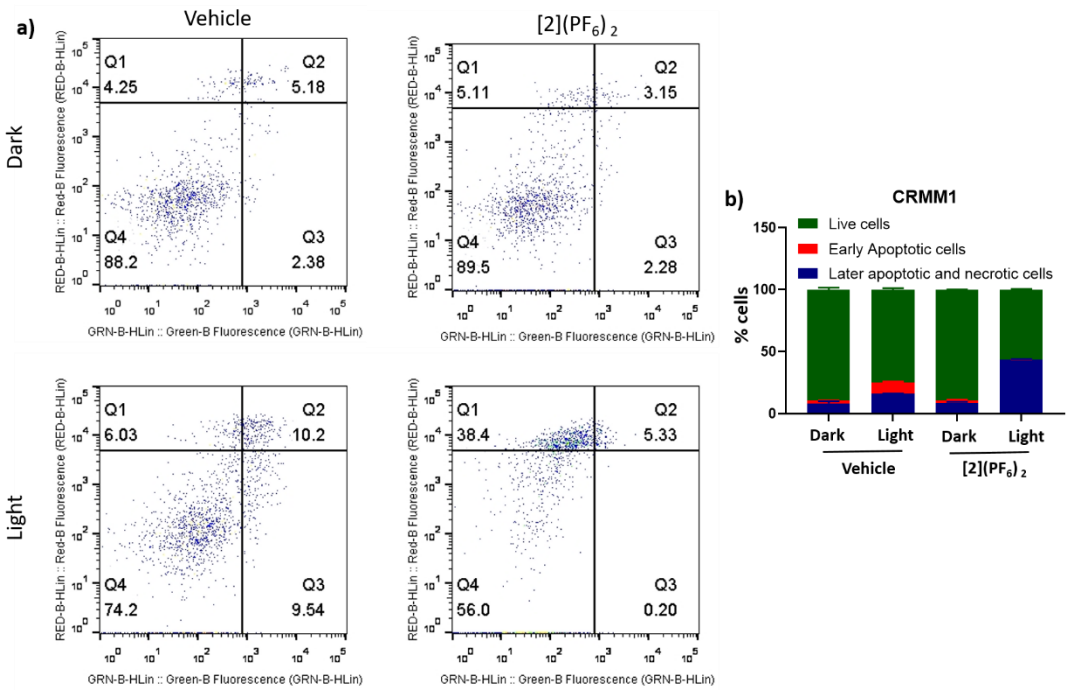

Figure S3 Green light irradiation of [**2**]$(PF_6)_2$ induces apoptosis and necrosis in CRMM1 cells. 4.3 µM of [**2**]$(PF_6)_2$ was added into the medium of CRMM1 cells. After 24 h, [**2**]$(PF_6)_2$ was washed by new free-drug medium and 15 min of green light (21 mW/cm^2, 19 J.cm^{-2}, 520 nm) was performed. After treatment, the cells were incubated for another 48 h. **a)** CRMM1 cells were stained with Annexin-V-FITC and Propidium Iodide. **b)** The percentages of live, early apoptotic, later apoptotic and necrotic cells in CRMM1 were counted by FACS. Results are presented as means ± SD from three independent experiments.

MAXIMUM TOLERATED DOSE DETERMINATION

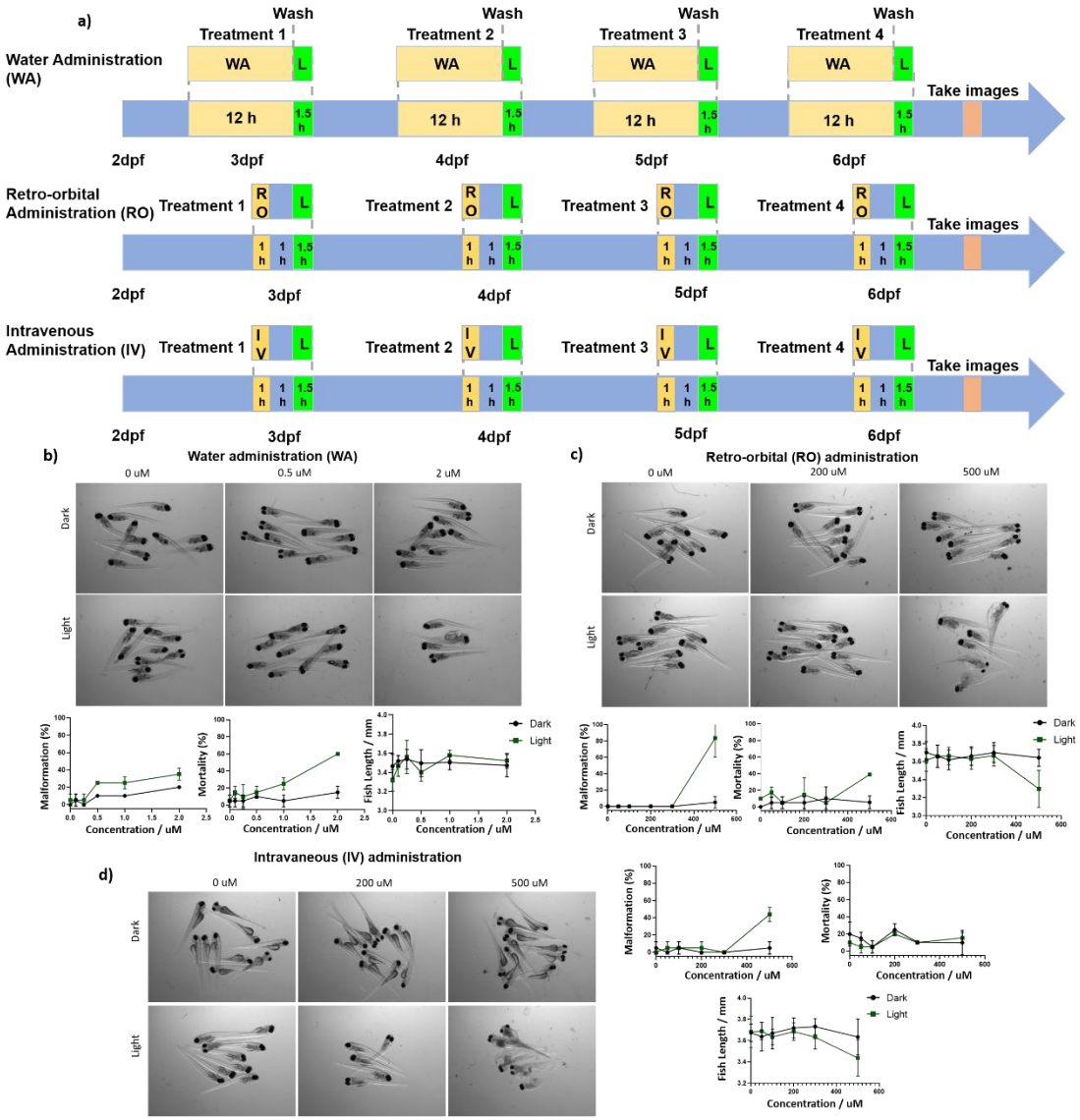

Figure S4 The maximum tolerated dose of [**2**](PF$_6$)$_2$ in wild type zebrafish embryos administered through three different routes. **a)** Schedule of [**2**](PF$_6$)$_2$ treatment in wild type zebrafish. Water administration (WA): [**2**](PF$_6$)$_2$ (0 µM, 0.1 µM, 0.25 µM, 0.5 µM, 1 µM, 2 µM) were added to the water containing 10 embryos per well at 2.5, 3.5, 4.5, 5.5 dpf, for 12h (yellow box). After these treatments, the drug was removed and replaced by egg water followed by 90 min green light irradiation (21 mW/cm^2, 114 J.cm^{-2}, 520 nm), depicted as a green lightning bolt. Intravenous injection (IV) or retro-orbital injection (RO): 1 nL of [**2**](PF$_6$)$_2$ (0 µM, 50 µM, 100 µM, 200 µM, 300 µM, 500 µM) were injected into the embryos at 3 dpf to 6 dpf every morning, followed by 60 min drug-to-light interval (yellow box) and 90 min green light irradiation (21 mW/cm^2, 114 J.cm^{-2}, 520 nm), depicted as a green lightning bolt. **b)** WA, c) RO, d) IV. **b-d)** Images were made of irradiated (light) and non-irradiated (dark) embryos (n=30) at 6dpf and the percentages of mortality, malformation and fish length were calculated (shown as means ± SD from three independent experiments). Representative images of embryos under dark and light conditions are shown.